Semiconductor Germanium and Germanium-Tin Thin Films by Simultaneous Laser Sintering and Crystallization

By

Md Toriqul Islam

A Thesis

Submitted to the graduate faculty of The University of Virginia,
in partial fulfillment of the requirements for the degree of
Master of Science in Electrical Engineering

Charlottesville, Virginia

2021

Semiconductor Germanium and Germanium-Tin Thin Films by Simultaneous Laser Sintering and Crystallization

Md Toriqul Islam

Abstract

The crystallization process of germanium (Ge) and germanium-tin (GeSn) thin films by a continuous wave (CW) and a pulsed laser is very effective for producing smooth, homogeneous, and crack-free polycrystalline films to use in transistors, photodetectors, and photovoltaic applications. However, little progress has been made to directly crystallize Ge and GeSn films based on micro/nanoparticles (NPs) using the laser sintering (LS) process. In this thesis work, a simultaneous LS and crystallization process of Ge and GeSn micro/nanoparticles thin films on silicon substrates are demonstrated. Silicon substrates with a silicon dioxide (SiO_2) insulating layer on top were considered for compatibility with complementary metal-oxide-semiconductor (CMOS) technology. The LS process was applied to solution deposited film of micro/nanoparticles, of 4-5 µm in thickness of Ge and GeSn using both CW infrared (IR) laser of wavelength 1070 nm and pulsed ultraviolet (UV) laser of 355 nm wavelength. After the LS process, around 2-2.5 µm thin films of polycrystalline Ge and GeSn were achieved with optical and electrical properties comparable to traditionally deposited films. The crystallinity of the polycrystalline Ge and GeSn films was evaluated by Raman spectroscopy and X-Ray diffraction (XRD). The laser-sintered Ge films exhibited a Raman peak at 300 cm^{-1} and XRD 2θ peak at 27.35, which indicated the poly-crystalline structure. The fabricated Ge film showed high hole mobility of 203 cm^2/V.s, without any doping and film electrical resistivity value of $6.24x10^5$ Ω-cm. The mobility increased after incorporating 12% Sn in the film. The laser-sintered GeSn films showed hole mobility of 240 cm^2/V.s. The developed LS process allows the quick deposition of thick polycrystalline films, removing surface porosity and voids, increasing films adhesion with the substrate, and faster thermal annealing.

Keywords: polycrystalline, Ge, GeSn, nanoparticle, laser sintering, crystallization, mobility, photodetector.

Acknowledgments

I would like to express my deepest appreciation to my advisor, Prof. Mool C. Gupta. I am extremely grateful for the guidance and support he provided in my master's program. I have learned a lot from his passion for research, deep thinking, rigorous attitude, and supportive mentoring style, which would be incredibly valuable in my future research/career life. I would also like to convey my gratitude to my committee members, Prof. Andreas Beling and Prof. Kyusang Lee, for the insightful comments and suggestions in the dissertation process. A special thanks to the thesis advisor, Dr. Mool C Gupta, for providing the opportunity and guidance to successfully carry out this thesis research.

I would also like to acknowledge the support of the National Science Foundation (NSF), NASA Langley professor program, and the Industry-University Cooperative Research Centers (IUCRC) program. Thanks to all Nanoscale Materials Characterization Facility (NMCF) and Microfabrication Laboratories.

Table of Contents

List of Tables

List of Figures

List of Abbreviations

Ge	Germanium
Sn	Tin
CW	continuous wave
NPs	nanoparticles
NCs	nanocrystals
LS	laser sintering
UV	ultraviolet
CMOS	complementary metal-oxide-semiconductor
IR	infrared
MEMS	micro-electromechanical system
SPC	solid-phase crystallization
MIC	metal-induced crystallization
CVD	chemical vapor deposition
MBE	molecular beam epitaxy
TFTs	thin-film transistors
FPA	focal plane array
SPE	solid phase epitaxy
PLD	pulse laser deposition
PLA	pulsed laser annealing
RTA	rapid thermal annealing
SEM	scanning electron microscopy
EDX	energy dispersive X-ray
XRD	X-Ray diffraction
ZrO_2	zirconium oxide
SiO_2	silicon dioxide
BK7	Borosilicate crown glass
FWHM	full width half maximum

ALD	atomic layer deposition
IPCs	Integrated photonic circuits
GeO_2	germanium oxide
SnO_2	tin oxide
Al_2O_3	aluminum oxide
D_{it}	interface defect density
Q_f	fixed charge density
S_{eff}	surface recombination velocity
W	Watts
D*	Detectivity

Chapter 1. Introduction

1.1. Group IV Material Overview

The crystalline semiconductors offer superior electrical and optical properties compared to their amorphous counterpart, which is a key requirement for optoelectronic applications. Developing crystallized semiconductor thin films on different substrates requires a complex fabrication process. Si-based materials are the main driving force behind the rapid development of revolutionary electronic technology. However, this technology is going to a phase of slow growth approaching the "Moore's law" limit. Also, Si is an indirect bandgap material that is not suitable for optoelectronic devices. The group IV photonics is getting significant momentum for future optoelectronics. It can be fabricated using the standard semiconductor fabrication techniques and integrated with high-speed microelectronic chips. Among the group IV materials, Ge and Sn are recently getting a lot of attention for next-generation optoelectronic devices. Ge is an indirect bandgap semiconductor that can be transformed into a direct bandgap semiconductor by incorporating Sn.

1.2. Ge Semiconductor

High-quality polycrystalline Ge thin-film material is of great interest for next-generation IR-sensitive material due to the lower bandgap [1], [2], good compatibility with Si [3], non-toxic and environmentally friendly green material [4], larger Bohr exciton radius (24 nm) [4], and high carrier mobility (340 $cm^2/V.s$) [3], [5], [6]. Ge is considered the best candidate for the near-IR spectral range photo-detection due to its high absorption coefficient for 1.3-1.55 μm wavelength range [2], [7]. Furthermore, mobility can be increased by incorporating tin (Sn) in the film [8]. However, there is a huge fabrication challenge of integrating Ge with Si due to a large lattice mismatch of 4.2% [9]. The Ge thin films of microns in thickness are used for micro-electromechanical systems (MEMS) [10], gas sensors [11], [12], and integrated photonic devices [13]–[17], as well as for single-photon avalanche diode detectors [18]–[20].

1.2.1. Ge thin film fabrication challenges

The polycrystalline Ge thin film is usually fabricated by using a costly and time-consuming process such as solid-phase crystallization (SPC) [3], [21], [22], metal-induced crystallization (MIC) [22]–[24], and chemical vapor deposition (CVD) [25], The SPC process requires 5-10 hours of thermal annealing at a very high temperature of around 500 °C [1]. The high annealing temperature is not suitable for all types of substrates. The MIC offers low-temperature processing but causes metal contamination in the films [1]. These traditional methods also have a requirement of very high-end vacuum-based deposition. Traditional methods have a slow deposition rate, which limits the thickness of the film and produces large amounts of hazardous waste. Also, it is very challenging to deposit thin films (i.e., 3 μm or more) by conventional fabrication methods.

1.2.2. Ge thin film fabrication prospects by laser

Recently, the LS crystallization of thin films is getting popular due to its ability of rapid recrystallization at low substrates temperatures and high energy throughput [26]. The usage of laser is increasing rapidly in thin-film fabrication, including contact patterning, selective etching, and surface micro texturing [27]. Both CW [5] and pulse laser [1], [6] have been used for fabricating high-quality crystallized thin films. The pulsed laser sintering presents versatile control for the fabrication of polycrystalline films [1]. The laser sintering of micro/nanoparticles provides a continuous film and simultaneous crystallization of thin film. The LS method of crystallizing films is a cost-effective, fast, scalable, and low thermal-budget process than furnace-based processes [9]. However, most of the published LS-based scientific reports used complex deposition methods such as CVD [9], molecular beam epitaxy (MBE) [5], and plasma sputtering [6]. Also, the thickness of the film is limited to a maximum of 1 μm. Additionally, the mobility of the polycrystalline Ge film is low without p/n-type doping. Researchers tried to synthesize Ge NPs by laser ablation from pure Ge target submerged in water [28]. Some also have reported laser melting of Ge NPs, but to our knowledge, no results have been reported on simultaneous laser sintering and crystallization as a one-step process.

1.3. GeSn Semiconductor

Most recently, IR photodetectors based on GeSn alloy are being researched and used due to their outstanding electrical and optical properties. The GeSn alloy can be transformed from indirect to direct bandgap with a wide range of Sn ratios incorporated in Ge [29], [30]. Usually, InGaAs-based photodetectors are used for photodetection in the short and mid wavelength IR (1–3 μm), which are incompatible with Si and require expensive bonding to readout silicon circuits to achieve IR imaging sensors [31]. Direct bandgap materials are preferred for optoelectronic applications. The wide applications of GeSn thin films are already successfully realized, such as thin-film transistors (TFTs) [32], p-MOSFETs on Si [33], and GeSn lasers [34], [35].

1.3.1. Properties of GeSn semiconductor

The unique properties [2], [8] of GeSn alloy allow it to use as photodetector materials, especially in the IR range. The properties are summarized as below:

i. Strain-relaxed and low threading-defect densities
ii. Low growth temperatures and thermal stability for semiconductor processing
iii. Tunable energy bandgap (0.5-0.8 eV) and lattice constants (5.65-5.8 Å)
iv. Low surface roughness
v. Compatible with Si and Ge substrate
vi. Easy chemical cleaning for subsequent ex-situ epitaxy
vii. Compatible with CMOS technology
viii. Suitable for focal plane array (FPA) integration
ix. Low-power operation.

1.3.2. The current state of GeSn based photodetectors

A list of GeSn photodetectors is summarized in a recent review paper [8], which mostly used CVD [36], [37], and MBE [38]. MBE fabrication process relatively costs higher than the CVD process. Both of these processes have limitations of depositing thick films and controlling the amount of Sn ratio. Other fabrications methods such as solid phase epitaxy (SPE), sputtering, and pulse laser deposition

(PLD) [39]–[42] also have been experimented with. However, incorporating Sn in Ge is a significant fabrication challenge as the material is unstable at high Sn concentration due to the low solubility limit of below 1%, the large lattice mismatch (~14.7%), and the strong surface segregation of Sn in Ge [30], [38]. This hinders the development of high-Sn content GeSn thin films. Despite the manufacturing complexities, the GeSn alloy is a promising material for future photodetector applications due to its outstanding characteristics.

The photodetector device structure mostly follows the p–i–n configuration. The reported devices have the highest detectivity (D*) [43] of $4.6x10^{9}$ $cmHz^{1/2}W^{-1}$ and responsivity [36] of 2.85 AW^{-1} at 1.55 µm wavelength. Both single-crystal [44]–[46] and polycrystalline [47]–[49] GeSn thin films are reported for photodetection. The absorption coefficient of the polycrystalline form is higher than the single crystalline because of the scattering effect at the grain boundaries. However, the electrical resistivity of the single crystalline form could be higher than the polycrystalline form because the grain boundaries generate holes in Ge-based semiconductors.

1.3.3. GeSn thin films by laser sintering

Researchers are trying to overcome fabrication challenges by extensively using non-equilibrium techniques. One of the most prominent ways is to use pulsed laser annealing (PLA) to synthesize GeSn alloy with strong control over Sn ratio [31], [39]–[41], [50]. Crystallization through laser annealing is getting attention due to its ability to rapid recrystallization during the LS process. The LS process provides a source of local and rapid annealing and then cools down in nanoseconds time scale, which is very much shorter compared to rapid thermal annealing (RTA) [48]. The GeSn material can be designed to become a direct bandgap group IV semiconductor by controlling the ratio of Sn. Usually, Ge has considerably higher carrier mobility compared to Si and the ability to combine with other materials such as Sn [30]. The responsivity of the GeSn photodetectors shifts into the IR region with the higher Sn content [38]. The laser sintering offers a cost-effective method to deposit polycrystalline GeSn films with high Sn content.

Table 1 shows a list of developed GeSn thin films on different substrates by using mostly UV laser [39]–[42], [48], but it also includes a costly MBE process. However, papers only reported crystallization through laser annealing and analyzed the morphological structure of the developed films. So far, no group has reported any electrical or optical properties of the laser deposited films.

Table 1: GeSn thin-film development by Pulsed Laser Annealing (PLA)

Crystal Structure	Fabrication	Sn (%)	Thickness (nm)	Substrate	Laser used	Ref
Epitaxial Alloy	MBE and PLA	5	200	Ge/n-Si	Nd:YAG, λ: 1064 nm	[31]
Polycrystal	MBE and PLA	12-14	100	Quartz	KrF excimer, λ: 248 nm	[39]
Epitaxial Alloy	MBE and PLA	1	40	Si	ArF excimer, λ: 193 nm	[40]
Polycrystal	MBE and PLA	2	50	SiO_2/Si	KrF excimer, λ: 248 nm	[41]
Epitaxial Alloy	Sputtering and PLA	22	100-1000	Glass, InP, ZnSe	UV (ArF & KrF)	[42]
Polycrystal	Sputtering and PLA	10-18	400	Ge	KrF excimer, λ: 248 nm	[48]
Epitaxial Alloy	MBE and PLA	1	100	v-Ge/Si	ArF Excimer, λ: 193 nm	[50]

1.4. Thesis Statement

In this thesis, we describe the deposition of Ge and GeSn thin films using Ge and Sn NPs by a centrifuge deposition method, subsequent LS processing, and simultaneous crystallization. This experimental work was targeted to establish a method to deposit both Ge and GeSn thin films around 2.5 μm thickness with high carrier mobility. The surface morphology, optical, and electrical properties of the fabricated film were characterized using different methods such as scanning electron microscopy (SEM), Raman spectroscopy, optical absorption, XRD, and Hall measurement. This study mainly focused on increasing hole mobility of thin polycrystalline Ge films by LS process and the dependence of carrier mobility on laser power density. Additionally, this study focused on incorporating Sn in the Ge for fabricating GeSn thin films to further enhance mobility. The micro-Raman spectra and XRD peaks have been analyzed in detail to verify the polycrystalline nature of the films. We have achieved a high mobility value of 203 cm^2/V.s for Ge thin films and 240 cm^2/V.s for GeSn thin films. These high hole mobilities were achieved through the LS process without any p/n-type doping. The LS method

allowed us to achieve Ge and GeSn thin films in the micron-scale thickness using a rapid deposition and sintering process. We introduced a way of directly melting the NPs of different materials by using the LS process. Finally, we present a fundamental understanding of the laser crystallization process and improvements in hole mobility. The fabrication method used in this experiment is also applicable to a variety of other materials and allows for large-area device fabrication.

Chapter 2. Experiments: Fabrication and Characterization

2.1. Fabrication

The polycrystalline Ge and GeSn thin film fabrication process consists of a few steps, as shown in figure 1, which are ball-milling, nanocrystal solution preparation, substrate cleaning including plasma treatment, centrifuge deposition, and laser sintering. The Ge and GeSn microparticles were ball-milled to attain NCs solution, then deposited on pre-cleaned substrates using centrifugal force. Finally, the deposited films were laser sintered to produce dense crystallized films. Each of the steps is discussed briefly in the following section.

Figure 1. Schematic representation of the Ge and GeSn thin films fabrication process.

2.1.1. Ball milling and nanocrystal solution

The Planetary Ball Mill model, Retsch PM100, was used for the fabrication of nanoparticles. A zirconium oxide (ZrO_2) milling cup was filled with a 3 mm diameter of ZrO_2 balls by 50% volume. Both cups and balls were chosen from the same ZrO_2 material to avoid contamination during the milling process. Wet milling is a key step to make uniform particle size distribution and maintain zero hazardous waste. Ball milling time, speed, and cooldown intervals were chosen carefully to avoid excessive heat buildup. Ge NPs of 0.5-0.8 µm average sizes and Sn NPs of 0.3-0.5 µm average sizes were purchased from Nanostructured & Amorphous Materials Inc with 99.99% purity.

2.1.1.1. Ge nanocrystal solution

The process started with ball milling of 0.5 g of Ge particles, which were wet-milled to produce nanocrystals (NCs) suspended in 25 mL of methanol solution. The Ge NPs were wet-grinded with methanol solvent to reduce the particle size distributions. Ball milling was run for a total of 2 hours with 10 mins break time after every 20 mins of running at 400 rpm. After ball milling, the concentrated NCs solution was transferred to a glass beaker of 50 mL size. Then the solution was diluted into a total of 25

mL solution and ultrasonicated for 5 to 10 mins to obtain a uniform dispersion. The ball milling process can be eliminated if Ge nanoparticles are purchased with uniform size distribution.

2.1.1.2. GeSn nanocrystal solution

Ge and Sn weight ratio was chosen based on the atomic ratio to obtain an approximate atomic percentage. Two different types of solutions were prepared for the 2% and 15% Sn ratio in GeSn. At first, for 98% Ge and 2% Sn atomic ratio, 0.33 g Ge and 0.02 g Sn weight ratio were weighted. Secondly, for 85% Ge and 15% Sn atomic ratio, 0.25 g Ge and 0.10 g Sn weight ratio were weighted. Both mixtures were wet pasted separately in a methanol solution. The wet-solution procedure is very effective in avoiding air dust and wastage. For the 2% Sn ratio, the ball milling time was the same as Ge only. Ball milling was run for a total of 2 hours at 400 rpm with 10 mins break time after every 20 mins. For the 15% Sn ratio, the total effective ball milling time was the same, but the intervals were different to avoid heat build-up and oxidation. Ball milling was run for a total of 3 hours at 400 rpm with 20 mins break time after every 20 mins. After ball milling, the concentrated NCs solution was taken out, and a total of 35 ml of the diluted solution was prepared and well mixed using an ultrasonication probe for 10 minutes. This mixing process is a crucial step to make uniform particle size distribution and maintain zero hazardous waste.

2.1.2. Wafer cleaning and plasma treatment

An <100> orientation silicon substrate of 500 µm thickness with thermally grown 2 µm SiO_2 was purchased from the University Wafer Inc. This wafer was selected for this experiment because the SiO_2 insulating layer allows measuring accurate electrical characteristics as it isolates the film from the Si substrate. The 10 cm diameter-sized wafer was cut into 1×2 cm rectangular pieces. Each piece was cleaned using the standard RCA process to remove organic residue from the wafer. Specifically, three steps of wet cleaning were carried out, which are acetone, isopropanol, and DI water. A plasma treatment was followed by the wet cleaning steps to remove contamination and hydrocarbons from the wet cleaned wafer surface [51], [52]. Plasma cleaning is a very effective and environmentally safe method for critical surface preparation. In addition to the cleaning, plasma cleaning produces a pristine surface, ready for bonding, without any harmful waste material.

2.1.3. Film deposition

After cleaning, each piece was placed in a vial (20 mL) filled with 4 mL of pure methanol. For Ge film deposition, 1 mL of Ge NCs diluted solution was used. For GeSn film deposition, 400 µL of GeSn NCs diluted solution was used. The sealed vials were placed in a centrifuge and spun at 100 rpm for around 15 mins. After centrifuge, the solution is transparent, leaving a dense and compact film on substrates at the bottom of the vial. The clear solvent is carefully removed from the vials using a micro-pipette. Then the films are dried on a hot plate at 70-80 °C for 2-3 mins to get rid of organic residues. The thickness of the as-deposited Ge film was around 5 µm, which was reduced to around 2.5 µm after the LS process. The thickness of the as-deposited GeSn film was around 4 µm, which was reduced to around 2 µm after the LS process.

2.1.4. Laser sintering (LS)

All the LS processes were done in a vacuum chamber purged with non-reactive (argon or nitrogen) gas to avoid oxidation of the film. The vented chamber consists of an inert gas inlet, a vacuum outlet, and an open window. The gas inlet is used for purging non-reactive gas into the chamber. The vacuum outlet is used for taking out the air molecules and non-reactive gas coming from the gas inlet. The vacuum outlet also helps to carry out the ablated material from the chamber during the LS process. The open window was closed by a Borosilicate Crown (BK7) glass purchased from Edmunds Optics to allow laser rastering on the sample. The BK7 glass window was chosen because it allows high transmission (above 95%) throughout the visible and near IR spectra and down to a wavelength of 350 nm in the UV. The as-deposited Ge or GeSn film was placed in the chamber. The laser, after passing through the galvo, entered the chamber through the BK7 glass. The substrate temperature during the LS process played a crucial role in controlling the film surface morphology.

Two different laser types were evaluated, a long pulse (100 µs) Nd:YAG fiber laser (IPG Photonics, YLR-150/1500) with a wavelength of 1070 nm and a solid-state diode-pumped short pulse (25 ns) UV laser (Coherent MATRIX) with a wavelength of 355 nm. The 1070 nm wavelength IR laser was used in both pulsed and CW modes, and the 355 nm wavelength UV laser was used in only pulse mode. Laser parameters such as repetition rate, scan speed, spot size, beam overlap, line-to-line overlap, and

power conditions were optimized to obtain a uniform recrystallized thin film. The detailed calculation process of the beam overlaps and the line-to-line overlaps were reported in our previous work [53].

2.1.4.1. Laser controlling parameters

Laser parameters were optimized to obtain a uniform recrystallized thin film. The detailed calculation process of the beam overlaps and the line-to-line overlaps were reported in our previous work [53]. The following laser parameters are the key for NPs sintering.

i. Repetition rate
ii. Scan speed
iii. Spot size
iv. Beam overlap
v. Line-to-line overlap
vi. Power

2.1.4.2. UV 355 laser sintering

In the UV laser (355 nm) crystallization process, the laser light is absorbed near the top surface of the film. This means that the UV laser starts melting the top surface as soon as it hits the film, and heat flows to the bottom with sufficient laser power and scan time to melt all the way to the substrate surface. So, perfectly optimized laser parameters are required to obtain a strong adhesion between substrate and film.

The optimized laser parameters for fabricating Ge films are the following: spot size ~100 μm, repetition rate ~30 kHz, scan speed ~50 mm/s, spot overlap ~60%, line scan pitch ~50%, and average laser power of 1.5 W. The laser repetition rate was selected at 30 kHz, where the pulse UV laser provides maximum peak power (operations manual of MATRIX 355-8-50, Coherent Inc.). The average power depends on the set current at which the UV laser was operated. For GeSn films, the same laser parameters were used except scan speed and laser power. These two parameters changed with the ratio of Sn in the GeSn film. Even a lower scan speed of 25 mm/s was used for GeSn films. The details are explained in the results section.

2.1.4.3. IR 1070 laser sintering

The 1070 nm IR laser in the CW mode with a Gaussian beam profile could provide a maximum power of 150 Watts (W). One of the key advantages of the IR laser is that it has a longer absorption depth. So, the IR laser can go through the top surface to heat the substrate, melt the substrate/Ge interface, and makes a strong adhesion between the film and the substrate.

At first, 450 µm spot size was selected based on our previous experience of crystallization and then optimized to 200 µm spot size for both Ge and GeSn films. For Ge films, a slow scan rate (10 mm/s) with moderately high power (30 to 35 W) was used to obtain sufficient laser energy absorption in the film for melting with minimal thermal stress. The laser line scan pitch was set to 60% to have sufficient overlaps between laser scan lines. The laser repetition rate was optimized to 500 Hz for efficient melting. High laser power and slow scan rate caused too much ablation and extreme substrate heating, which led to complete Ge film loss. Also, a high scan rate causes incomplete recrystallization and high thermal shock. So, optimized laser parameters are key to obtaining complete recrystallization of the Ge film. For GeSn films, all the optimized parameters as above were used except the power requirements. The required power to melt GeSn NPs is different from Ge only due to the ratio of Sn in the film. The details are explained in the results section.

2.2. Characterization Equipment

The fabricated Ge and GeSn films were evaluated using a set of characterization tools, which are listed below:

i. SEM model FEI Quanta 650: Microscopic surface morphology was determined using this model. Elemental analysis was performed using an energy dispersive X-ray (EDX) detector attached to the SEM, and data was later processed using Aztec software.

ii. Renishaw Raman spectrometer: Micro-Raman measurements were carried out with a 514 nm excitation (argon laser) source at room temperature.

iii. PANalytical Empyrean X-ray diffractometer: The X-ray diffraction (XRD) patterns were collected using Cu Kα as the source (λ= 0.154 nm).

iv. Hall measurement method: The hole mobility, carrier concentration, and resistivity were measured for both as-deposited and laser-sintered films in the van der Pauw configuration.

v. Cary UV-Vis-NIR Spectrophotometer: The optical transmission and reflection spectra were collected by using this instrument.

vi. Labsphere integrating sphere (RTC-060-SF): The total scattering and reflection loss was measured using this model.

Chapter 3. Results for Ge Thin films

3.1. Laser Sintering Impact on Surface Morphology

The surface morphology of as-deposited and laser-sintered Ge films with different laser conditions is shown in figure 2 to figure 4. The as-deposited micro/nanoparticle film surface is porous on a sub-μm scale with surface voids, as shown in figure 2 (a) due to variation of the particle size. Approximately 0.3–0.5 μm size particles are interconnected to form the Ge film. Laser parameters were carefully optimized to melt the particles, develop a continuous dense film, and recrystallize the film.

3.1.1. IR 1070 nm laser effect

The Ge film is a stronger absorber of 1070 nm IR light. At low power, the IR laser starts melting probably at the outer surface of the NPs. However, the power isn't enough to melt the NPs completely. As the power increases, most of the light is absorbed by the Ge NPs and partly transmits through the NPs to the substrate. This increases heat at the Si wafer and Ge interface, which yields to strong adhesion of the film with the substrate.

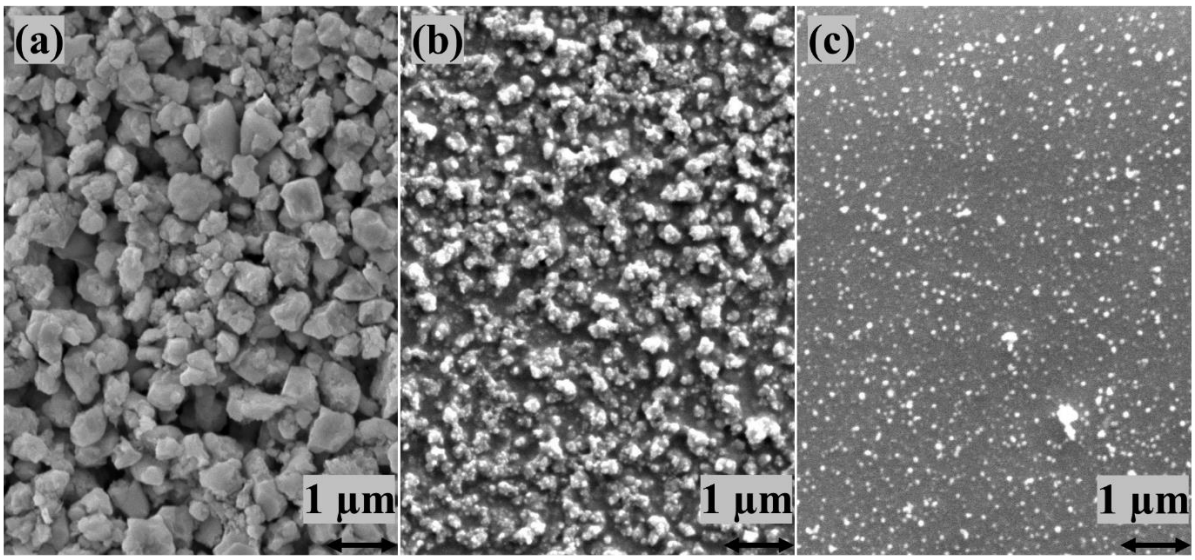

Figure 2. SEM images of surface morphology of as-deposited and IR laser-sintered Ge films with different laser parameters. (a) the as-deposited Ge film, (b) IR 1070 laser sintered between 20-25 W, (c) IR 1070 laser sintered between 30-35 W.

Figure 2(b) shows the IR laser condition where Ge NPs start melting, but power is not enough to melt all the NPs. Figure 2(c) shows the IR laser condition where Ge NPs completely melted and formed a uniform surface. The LS process not only removed the surface voids and porosity but also provided a dense and connected film. However, the substrate may crack and break if IR sintering is done with higher laser power than required due to high-temperature build-up in the Si substrate.

3.1.2. UV 355 nm laser effect

The UV laser starts melting from the top surface even at low power. The heat flows deep inside with increasing power. Figure 3(a) shows the UV laser condition where Ge NPs start melting from the top surface. Figure 3(b) shows the UV laser condition where Ge NPs completely melted from top to bottom and formed a consistent surface. However, a rough surface was generated when sintered with higher UV laser power than required due to high Ge NPs ablation, which is shown in figure 3(c).

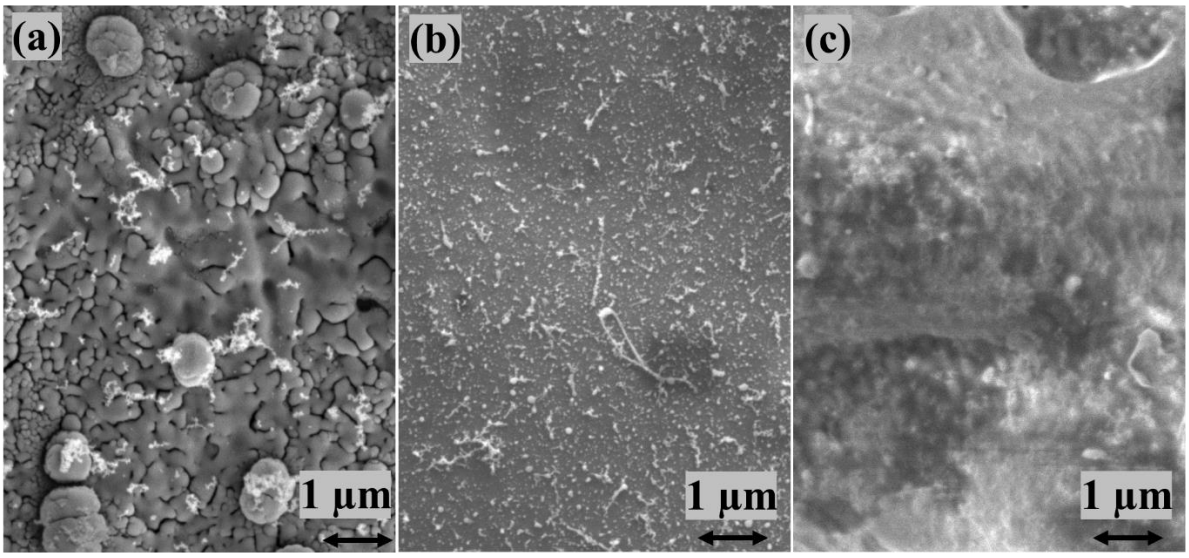

Figure 3. SEM images of surface morphology of UV laser-sintered Ge films with different laser parameters. (a) UV laser sintered at an average power between 0.5-1.0 W, (b) UV laser sintered at an average power of 1.5 W, and (c) UV laser sintered at an average power of more than 2.0 W.

3.1.3. IR and UV laser collective effect

An easier way to avoid substrate cracking and film ablation is to use both IR and UV laser together. The IR laser melts and develops a compact film but may have an uneven surface when considered large

area sintering. A subsequent UV laser sintering melts the top surface layer and creates a smooth surface. Figures 4(a)) and 4(b) show the laser-sintered films using both IR and UV laser together. This approach not only allows to avoid substrate cracking or film ablation but also reduces the surface roughness.

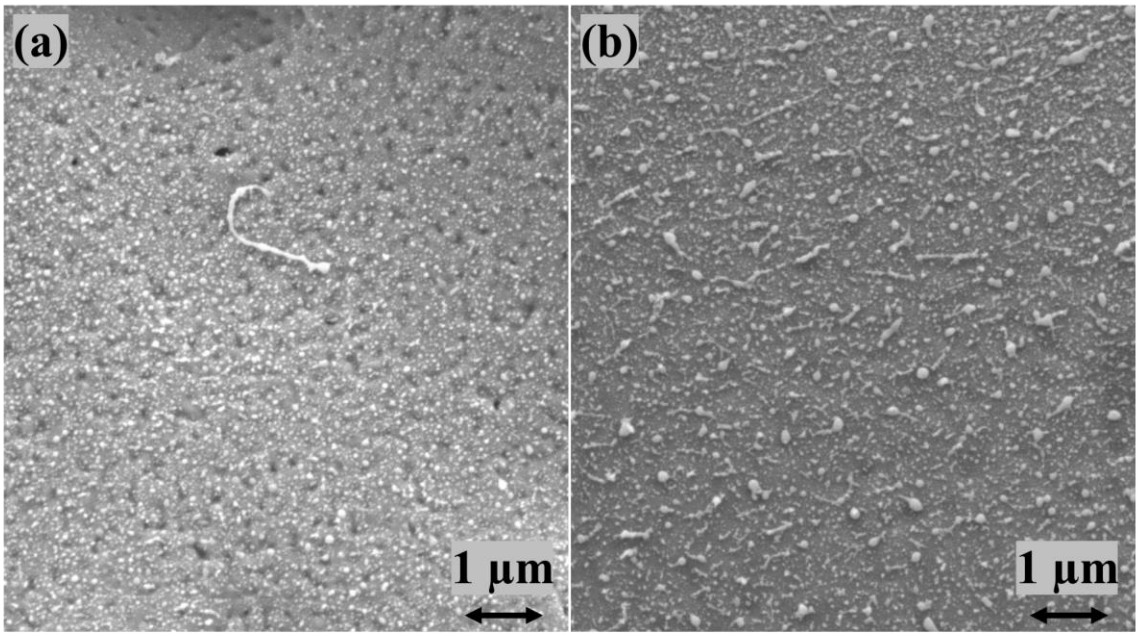

Figure 4. SEM images of surface morphology of IR and subsequent UV laser-sintered Ge films with different laser parameters. (a) IR 1070 laser sintered at 25 W and subsequent UV laser sintering done at an average power of 1.5 W, and (b) IR 1070 laser sintered at 25 W and subsequent UV laser sintering done at an average power of 2.0 W.

3.1.4. Ge film cross-sections

The SEM cross-sectional images of as-deposited and laser-sintered Ge films are shown in figure 5. Figure 5(a) shows as-deposited Ge films, where particles are interconnected to form the film. Still, it has large voids and poor adhesion to the substrate. The thickness of the as-deposited film is around 5 µm on top of a SiO_2 insulating layer. The LS process reduced voids in the film and increased substrate adhesion strength. Figure 5(b) shows the cross-section of IR laser sintered film at relatively medium power, where particles started melting and forming a dense film. If adequate power is used in IR sintering, then the films completely melted as shown in figure 5(c), and film thickness is reduced to 2 µm. Similarly, a UV laser was used to fully melt the film, as shown in figure 5(d). If IR and UV laser are used separately, then the achieved film thickness is around 2 µm. If IR and UV laser are combined,

then the achieved film thickness is around 2.5 µm, as shown in figure 5(e). When both lasers were used, less ablation occurred compared to the individual use of lasers at high power.

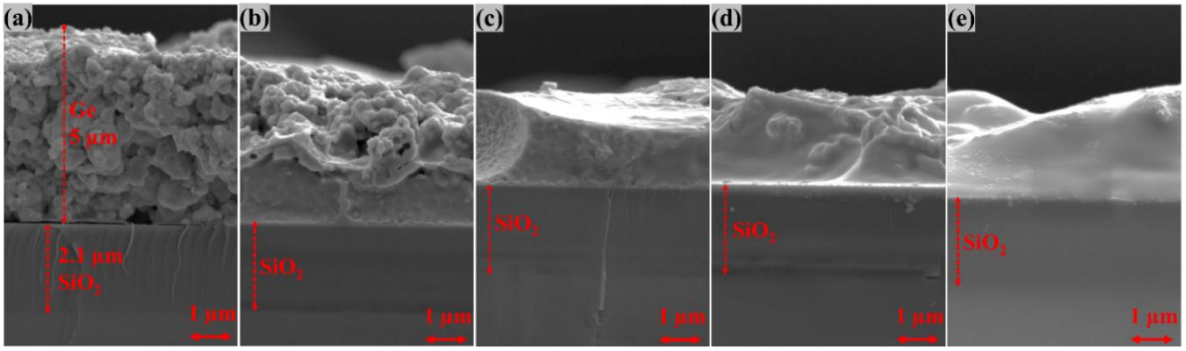

Figure 5. SEM cross-sectional images of as-deposited and laser-sintered Ge films with different laser parameters. (a) as-deposited Ge films, (b) IR 1070 laser-sintered between 20-25 W, (c) IR 1070 laser-sintered between 30-35 W, (d) UV laser-sintered with an average power of 1.5 W, and (e) IR 1070 laser-sintered with 25 W and subsequent UV laser-sintered with an average power of 1.5 W.

3.2. Elemental Composition

The as-deposited film showed 46% Ge and 54% oxygen, found by EDX analysis. It contains a high amount of oxygen due to the process involved in the Ge thin film fabrication. During the laser recrystallization process, the amount of oxygen is reduced from 54% to 43%, as shown below in figure 6. Thus, the amount of Ge increased from 46% to 57%. The reduction of oxygen may come from the film surface as the LS process starts melting and recrystallizing the films.

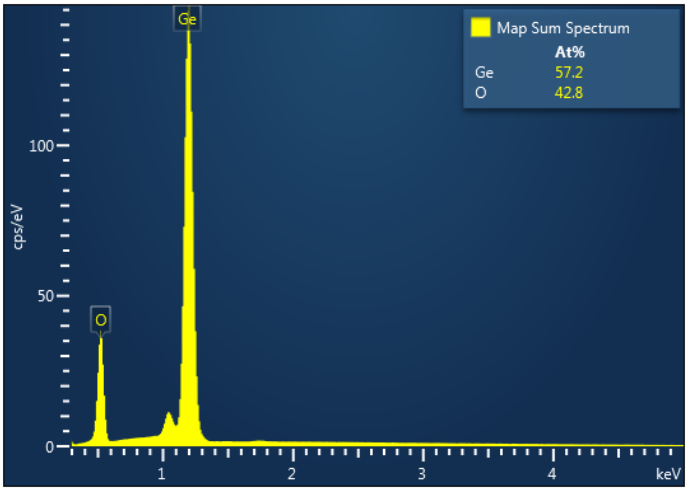

Figure 6. The typical EDX spectra of the laser-sintered Ge thin films.

3.3. Crystallinity Determination by Raman and XRD Measurements

Only IR 1070 laser sintered films were considered to better understand the physical impact of the LS process on the film properties.

3.3.1. Raman spectrum analysis

Raman spectrum for both as-deposited and laser-sintered films is shown in figure 7. Usually, the Raman peak of the bulk crystalline Ge due to Ge-Ge vibrational mode is observed at 300 cm^{-1} with symmetrical distribution at full width half maximum (FWHM) [4] of the peak position.

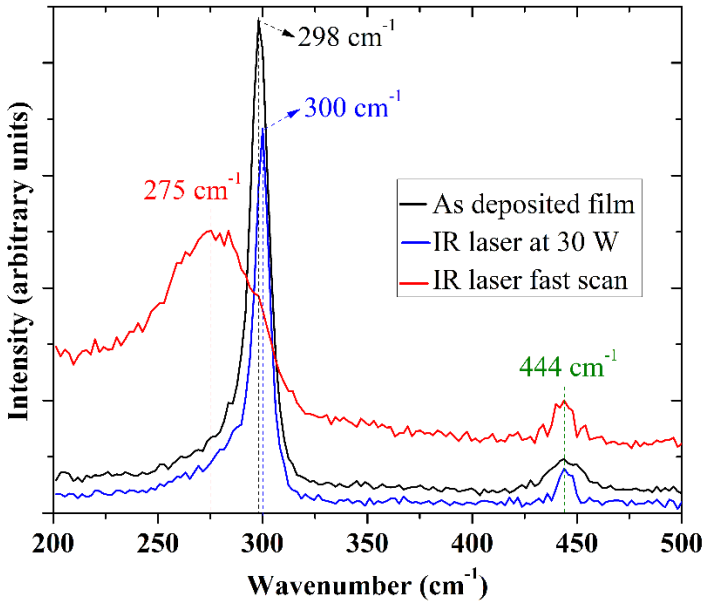

Figure 7. Raman spectra for the as-deposited and IR laser-sintered Ge thin films, measured by using a 514 nm laser excitation at room temperature.

The as-deposited Ge film showed a Ge-Ge vibrational mode peak around 298 cm^{-1}, as shown in figure 7 (black line). It shifted by 2 cm^{-1} from the standard crystalline Ge peak at 300 cm^{-1} due to the strain effect. The laser-sintered film with adequate power showed a sharp peak at 300 cm^{-1}, as shown in figure 7 (blue line). It also showed a much smaller FWHM compared to as-deposited film. It indicated that the laser-sintered Ge film was crystallized completely and showed polycrystalline nature. However, it is also possible to develop amorphous Ge (a-Ge) film by the LS process, as shown in figure 7 (red line). The LS process at high scan speed with the same power caused the formation of an amorphous phase due to fast cooling rates. The developed a-Ge film showed a broad spectrum with a wider peak

around 275 cm^{-1} and no peak at 300 cm^{-1}. The oxygen in the films plays a major role in this transformation. Also, the rapid heating and cooling of the film can generate the amorphous phase. Additionally, both as-deposited and LS processed films showed oxygen peaks around 444 cm^{-1}. This oxygen peak refers to GeO_2 formation, as reported in the literature [54], [55].

3.3.2. XRD peak analysis

The XRD patterns for both as-deposited and laser-sintered films are shown in figure 8. Films before and after laser crystallization demonstrated the same peak position. Two major peaks of germanium dioxide (GeO_2) were identified at a 2θ angle of 20.65° for GeO_2 (100) and 26.06° for GeO_2 (101), which are in alignment with the literature [56], [57]. The XRD peak of pure Ge was identified at a 2θ angle of 27.35° for Ge (111), 45.37° for Ge (220), and 53.71° for Ge (311), which indicates polycrystalline Ge films [57]–[60]. The peak position of Ge (111) is the same for both as-deposited and laser-sintered films. The intensity of the as-deposited film is low due to the high amount of oxygen and high porosity. The peak intensity at 27.35° increased by three to four times after the LS process due to the formation of Ge (111) orientation. This is also verified by EDX analysis, as shown in figure 6.

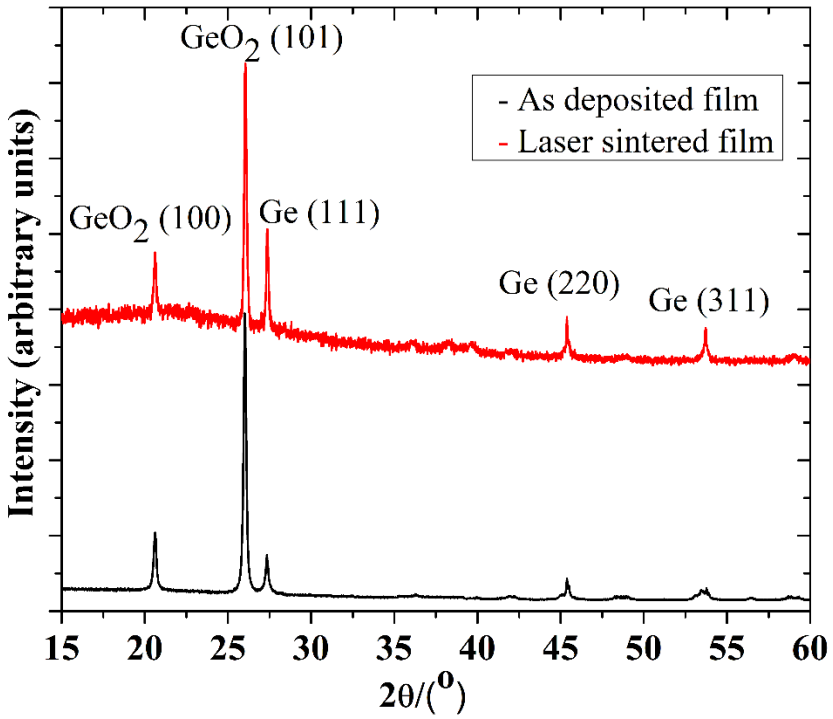

Figure 8. XRD patterns of as-deposited and laser-sintered Ge thin films.

3.4. Electrical Properties

Semiconductor devices on insulators with high-carrier mobility are important for optoelectronic applications. The carrier mobility of the semiconductor device depends upon the grain size of the fabricated films. This experimental work was aimed to achieve a high hole mobility Ge thin film without any dopant.

The hole mobility, carrier concentration, and resistivity of as-deposited Ge film were 43.9 $cm^2/V.s$, $2.08x10^{15}$ cm^{-3}, and $3.45x10^6$ Ω-cm, respectively. The hole mobility, carrier concentration, and resistivity of IR laser-sintered Ge film were 201.6 $cm^2/V.s$, $1.55x10^{15}$ cm^{-3}, and $6.24x10^5$ Ω-cm, respectively. The mobility of the sintered film increased by more than four times due to the recrystallization and melting effect by laser. Also, the resistivity of the film decreased by order of magnitude because the completely melted film had no voids or air gaps.

3.4.1. Mobility comparison with different fabrication methods

The recently reported hole mobility data of polycrystalline Ge film is summarized in Table 2. For better understanding and clarity, only hole mobility is considered. Watakabe et al. [6] first fabricated poly-Ge using laser annealing with boron (B) doping and reported mobility of 295 $cm^2/V.s$ Kasirajan et al. [61] reported a laser annealed poly-Ge sample, but the mobility is very low (52 $cm^2/V.s$). Usuda et al. [62] tried the flash lamp annealing process without doping and eventually achieved hole mobility of 200 $cm^2/$ V.s for poly-Ge MOSFET. Both Sadoh et al. [63] and Toko et al. [21] reported the same hole mobility (140 $cm^2/V.s$) for poly-Ge TFTs and poly-Ge thin films without doping. Toko et al. [3] reported maximum hole mobility (340 $cm^2/V.s$) for poly-Ge films using precursor-based MBE fabrication process and subsequent furnace annealing. Imajo et al. [58] experimented with the strain effect on poly-Ge thin films and eventually achieved 620 $cm^2/V.s$, hole mobility. High hole mobility can be achieved by either p-type doping or creating strain effects in the films. The thickness of these films varied between 50-400 nm. We are reporting here 2-2.5 μm poly-Ge thin films having a hole mobility of 203 $cm^2/V.s$. The films were fabricated using a simple centrifuge force and subsequent laser crystallization without using any doping.

Table 2. Hole mobility of polycrystalline Ge film fabricated and annealed by different methods with varying film thickness.

Fabrication process	**Substrate**	**Doping**	**Film type**	**Film thickness**	**Annealing method**	**Mobility, μ_h (cm^2/Vs)**	**Ref**
Centrifuge (our work)	SiO_2/Si		Poly-Ge	2-2.5 µm	Laser (UV and IR)	203	Current paper
Plasma sputtering	Quartz	B	Poly-Ge	50 nm	Laser (XeCl excimer)	295	[6]
CVD	SiO_2/Si		Poly-Ge nMOSFET	90 nm	Laser (UV and CO_2)	52	[61]
Sputtering	SiO_2/Si		Poly-Ge MOSFET	100 nm	Flash lamp in N_2	200	[62]
MBE+SPC	Glass		Poly-Ge TFTs	50 nm	500 ^{O}C for 3 h in N_2	140	[63]
MBE+SPC	Quartz		poly-Ge	50 nm	425-500 ^{O}C for 3 h in N_2	140	[21]
MBE+SPC	SiO_2 Glass	Precursor	Poly-Ge	100 nm	450 ^{O}C for 5 h in N_2	340	[3]
MBE+SPC	SiO_2, Si, Ge, Caf_2	Strain	Poly-Ge on GeO_x	400 nm	375 ^{O}C for 150 h in N_2	620	[58]

3.4.2. Mobility: LS process vs. furnace annealing

The mobility results of the IR laser-sintered film are also compared with the furnace annealed film, as shown in figure 9. The mobility of the IR laser-sintered film increases with the power of the laser, as shown in figure 9(a). The furnace annealed sample at 500 °C for ten hours showed mobility of 103.8 cm^2/V.s, as shown in figure 9(b). During the furnace annealing, the Ge film crystallizes. There could be an oxide growth on the surface of the film for longer time annealing, which may passivate the surface. Thus, the hole mobility increases in the furnace annealed films. However, Ge NPs don't melt completely

because of the high melting temperature of Ge (937.5 °C). This limits the hole mobility of the films due to the poor interconnection of Ge particles. The LS process is used to overcome this challenge. The maximum mobility was achieved by using the combination of both IR and UV laser, which was 203 $cm^2/V.s$ as shown in figure 9(a). It clearly shows that the LS crystallization significantly improves the hole mobility. The mobility of the furnace annealed sample is limited due to the surface voids and air gaps in the film. So, the furnace annealing requirement can be completely replaced by the LS and recrystallization process.

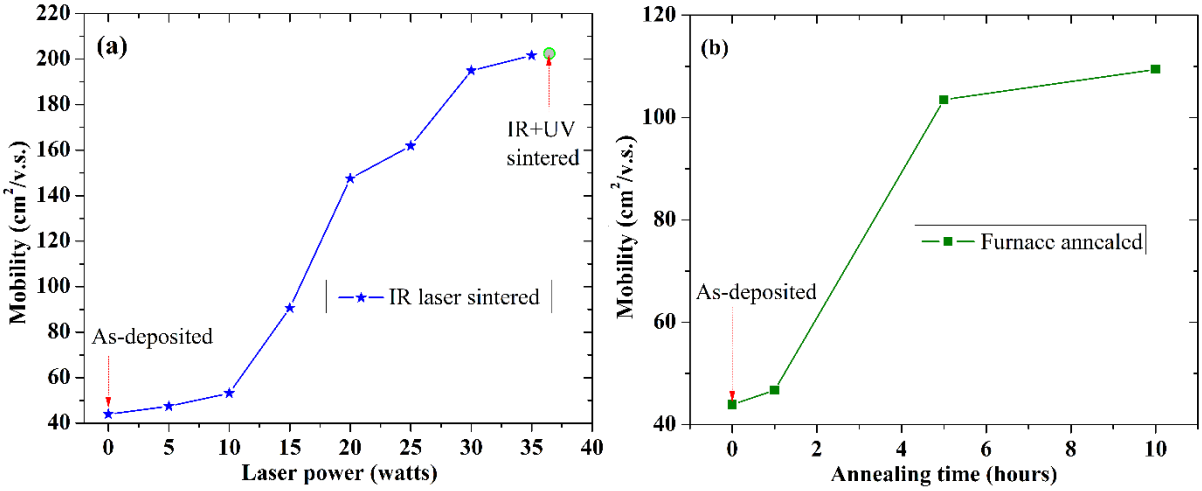

Figure 9. The mobility of Ge thin film, as a function of laser sintering power (a) and as a function of furnace annealing time at 500 ^0C.

3.5. Optical Properties

The optical transmittance spectra are shown in figure 10(a) for both SiO_2/Si substrate and Ge thin film. There is no transmission below 1000 nm of wavelength as expected since Si is used as substrate. The transmittance of the fabricated Ge thin film varies between 20-35% in the IR window (>1100 nm), which is very low. In other words, IR light is being absorbed by the thin Ge films, including some loss due to reflectance and scattering. Also, the oxygen in the film may cause less absorption of the light in the IR regime. Recently reported articles showed a high amount of IR transmission due to the smaller thickness of the films [64], [65]. The reflectance spectra are shown in figure 10(b) for both Si wafer and Ge thin film. There is around 2% reflection in the visible wavelength regime and 4-5% reflection in the IR wavelength regime. Scattering loss was also measured by using the Labsphere integrating sphere.

The total scattering and reflection loss is around 10-12% at a visible wavelength (i.e., 633 nm). It can be concluded that the laser-sintered film absorbs light more than 50% in the near to mid-IR regime with considering all the losses. Increasing IR light absorption will be very useful in photodetection applications.

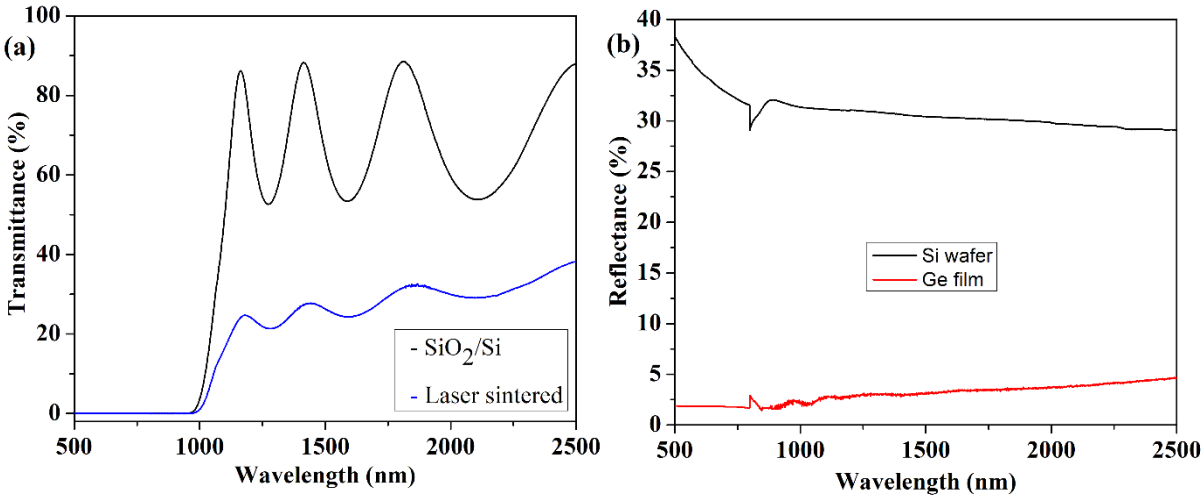

Figure 10. (a) The optical transmission spectra of the polycrystalline Ge thin film and SiO_2/Si substrate. (b) The reflectance spectra for both Si wafer and polycrystalline Ge thin film.

3.6. Discussion

The LS process offers a great advantage of simultaneous sintering and crystallization as a one-step method. The LS process can eliminate the porosity, and air gaps between NPs from the as-deposited films. Thus, it provides a dense and compact polycrystalline film having strong adhesion with the substrate. Both IR and UV lasers can be used separately to fabricate polycrystalline thin films. However, using only IR laser at higher power causes cracking of the substrate due to high-temperature gradients during sintering. The UV laser doesn't crack or break the substrate as it starts melting from the top. The UV laser sintering creates an uneven film surface. The extremely short melt duration does not produce a smooth surface as material flow is very limited. These problems can be overcome by choosing proper laser parameters of both IR and UV laser. Additionally, both lasers can be used at a medium power range, which is very effective for large area sintering.

During the LS process, the amount of oxygen in the film is reduced a little bit due to oxygen removal from the film surface. However, oxygen stays inside the film because of the rapid melting and

recrystallization. The strain introduced by ball milling during film deposition is removed by the LS process. This is verified by Raman spectra, which show a shift of 2 cm^{-1} from 298 cm^{-1} to 300 cm^{-1} for the Ge-Ge vibrational mode peak. Also, the FWHM becomes smaller, with a sharp peak at 300 cm^{-1} after the LS process. Additionally, the XRD analysis shows that the peak intensity becomes stronger after the LS process. Thus, the LS process is very effective in fabricating films with high crystal orientation. Moreover, the Ge thin film optical absorption can be increased by the LS process as the surface reflection is reduced and was measured as 10%. The film transmission was about 20-30%. Furthermore, the mobility of the laser-sintered film is almost doubled compared to the furnace annealed film due to the dense and compact film after the LS process.

The promise of Ge in optoelectronic applications is hindered by the high electronic defect density [66]. Surface passivation can be considered for mobility enhancement by reducing defects and the chemical reactivity of its surface. Berghuis et al. [66] showed the effect of aluminum oxide (Al_2O_3) passivation on Ge thin films prepared by atomic layer deposition (ALD). The surface passivation has two-fold effects. First, the ALD of Al_2O_3 on Ge leads to the formation of an ultrathin GeO_x layer between Ge and Al_2O_3. The remaining defects at the Ge/GeO_x interface are predominantly Ge dangling bonds, which leads to a low interface defect density (D_{it}). Second, Al_2O_3 yields a high negative fixed charge density (Q_f), which forms an electrical field. This phenomenon is known as field-effect passivation. The low D_{it} and high Q_f combination lead to low surface recombination velocity (S_{eff}). This eventually can increase the hole mobility of the films. The results reported in this study are without any surface passivation layer. So, further improvement in our hole mobility value could be realized by the appropriate surface passivation layer.

Chapter 4. Results for GeSn Thin films

4.1. As-deposited Films

The microscopic surface morphology SEM image of the as-deposited GeSn film is shown in figure 11. The as-deposited film surface is porous on a sub-μm scale (same as Ge films) and had particle size variations due to the different particle size distributions of Ge and Sn. Figure 11(a) shows GeSn film with a 2% Sn ratio, and 11(b) shows GeSn film with a 15% Sn ratio. Interestingly, the surface morphology is different for various Sn ratios. Both films were deposited using identical conditions, including the same ball milling time for NCs solution preparation. We found that if the atomic Sn ratio is below 5%, then it stays as particles, as shown in figure 11(a). However, it becomes more like flakes with a higher atomic ratio of Sn, as shown in figure 11(b). This phenomenon happens during the ball milling process. This mechanical alloying process results in flakes by intermixing Ge and Sn. These flakes are made of both Ge and Sn.

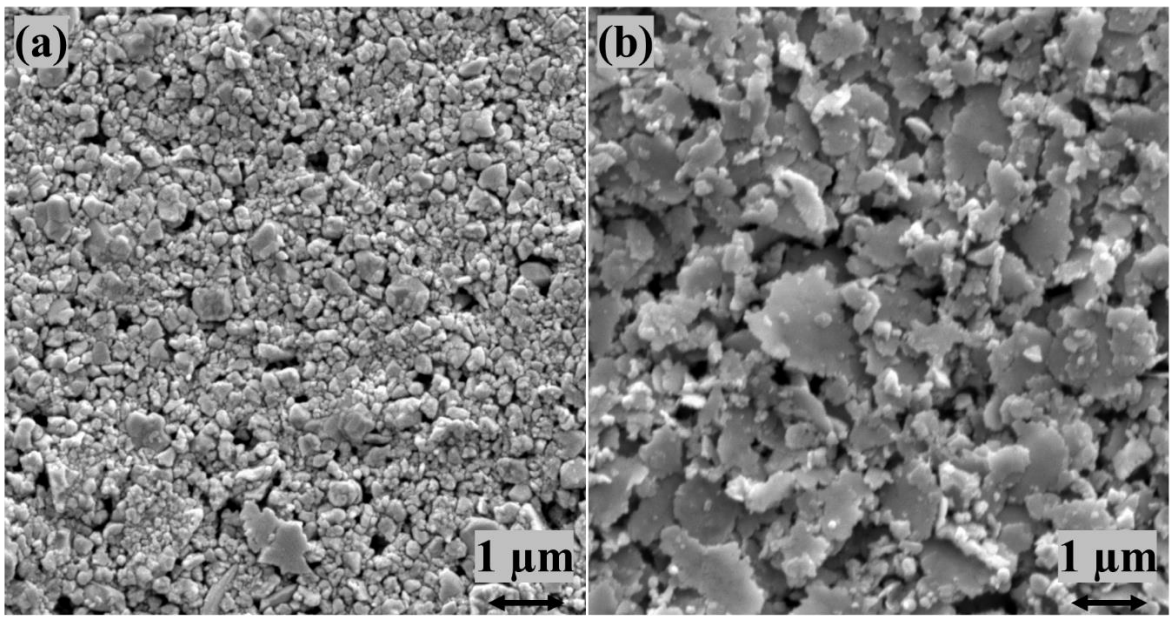

Figure 11. SEM images of surface morphology of as-deposited GeSn films. (a) 2% Sn ratio and (b) 15% Sn ratio.

4.2. Laser Sintering Impact on Surface Morphology

The surface morphology of as-deposited and laser-sintered (UV and IR) GeSn films with different laser conditions are shown in figure 12 to figure 14. Both UV and IR Laser parameters were carefully optimized to melt the particles and recrystallize the film for developing a continuous dense film. However, the surface morphology behaviors change with the ratio of Sn in the film, especially when sintered with a UV laser.

4.2.1. UV laser effect on $Ge_{0.98}Sn_{0.02}$ film

The UV laser starts melting from the top surface, as also shown for Ge films before. The increasing laser power helps heat to flow deep inside the film. However, the film surface is not as smooth as with only Ge films. Sn has the tendency of balling around during recrystallization. Figure 12(a) shows the UV laser condition (low power) where GeSn NPs start melting from the top surface. Figure 12(b) shows the UV laser condition (moderate power) where GeSn NPs melted and flattened to form a consistent surface. The surface becomes more flattened with increasing power adequately, which is shown in figure 12(c). Some GeSn NPs ablated during the melting and recrystallization process. GeSn NPs are completely melted and connected to form the film, but gaps are noticeable. This is due to the non-wetting nature of Sn, which causes the GeSn not to have enough wetting with the substrate. Substrate wetting during the LS process is a key requirement for uniform film deposition. It is still possible to get a uniform film with a low Sn percentage in the film, possibly below 5% Sn.

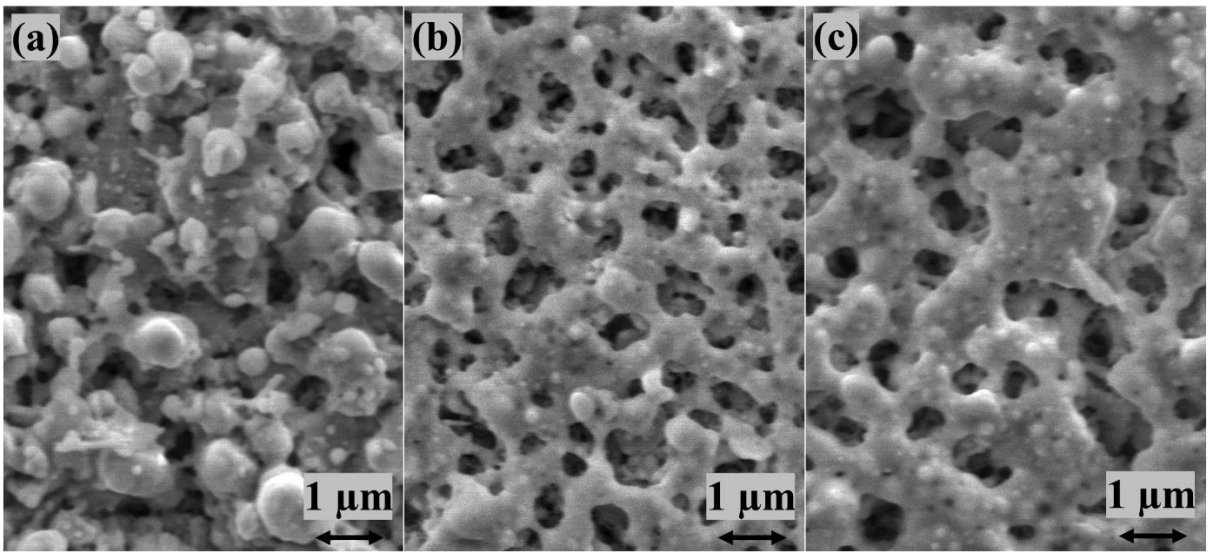

Figure 12. SEM images of surface morphology of UV laser-sintered GeSn films with 2% Sn ratio in the film. (a) UV laser sintered at an average power of 0.5 W, (b) UV laser sintered at an average power of 1.0 W, and (c) UV laser sintered at an average power of 1.5 W.

4.2.2. UV laser effect on $Ge_{0.85}Sn_{0.15}$ film

The Non-wetting effect of Sn is extremely noticeable with a high Sn ratio in the film, as shown in figure 13. Figure 13(a) shows the UV laser condition (low power) where GeSn NPs start melting but creating GeSn balls. Figure 13(b) shows the UV laser condition (moderate power) where GeSn NPs melted but did not flatten as expected due to high Sn concentration. Even though GeSn NPs are completely melted at adequate power, but they just formed large GeSn balls with no connection between them, which is shown in figure 13(c). The short pulse duration of the UV laser also causes this balling in addition to the non-wetting effect of Sn. Melted NPs don't get enough time to flow during recrystallization due to the very low pulse duration of the UV laser. These two folds effect limits the use of UV laser to form a continuous GeSn film with a high Sn ratio.

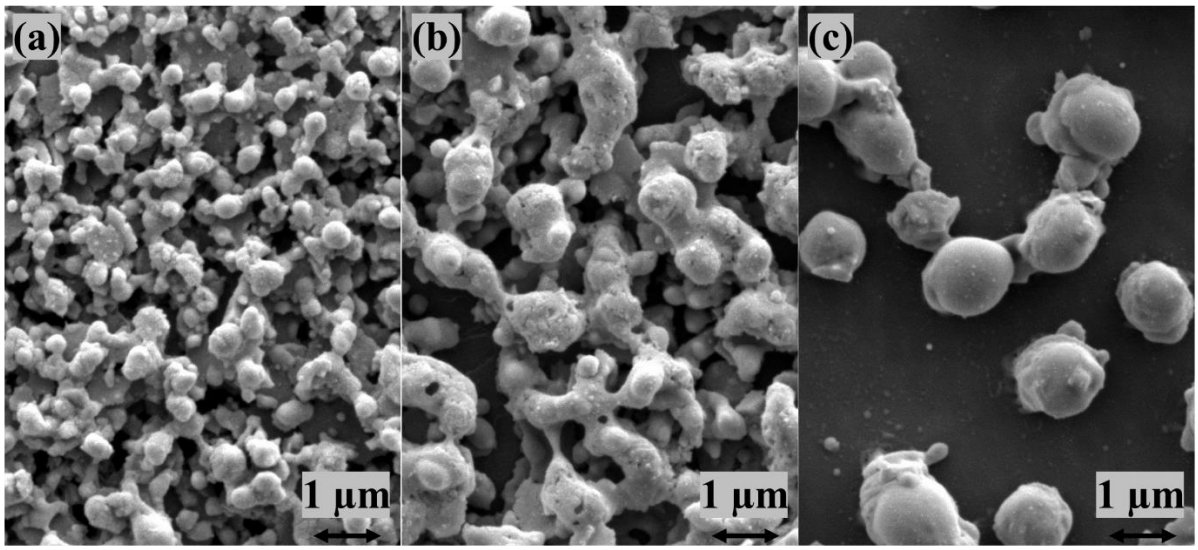

Figure 13. SEM images of surface morphology of UV laser-sintered GeSn films with a 15% Sn ratio in the film. (a) UV laser sintered at an average power of 0.5 W, (b) UV laser sintered at an average power of 1.0 W, and (c) UV laser sintered at an average power of 1.5 W.

4.2.3. IR laser effect on GeSn film

IR 1070 nm laser in continuous mode is considered to overcome the challenges faced in UV laser. In this mode, the GeSn NPs get enough time to flow and form a uniform film during melting and recrystallization. The impact of IR laser sintering on GeSn film is shown in figure 14. Figure 14(a) shows the IR laser condition where GeSn NPs start melting, but power is not enough to melt all the NPs. Figure 14(b) shows the IR laser condition where Ge-Sn NPs mostly melted and formed a uniform surface with a small balling effect. Figure 14(c) shows the IR laser condition where Ge-Sn NPs completely melted and formed a dense and connected film. Very small number of particles are seen on the surface, which comes because of the ablation. The IR LS process not only removed the surface voids and porosity but also solved the problem faced by the UV laser. The continuous mode of IR 1070 nm laser is proven very effective for GeSn films with a high Sn ratio.

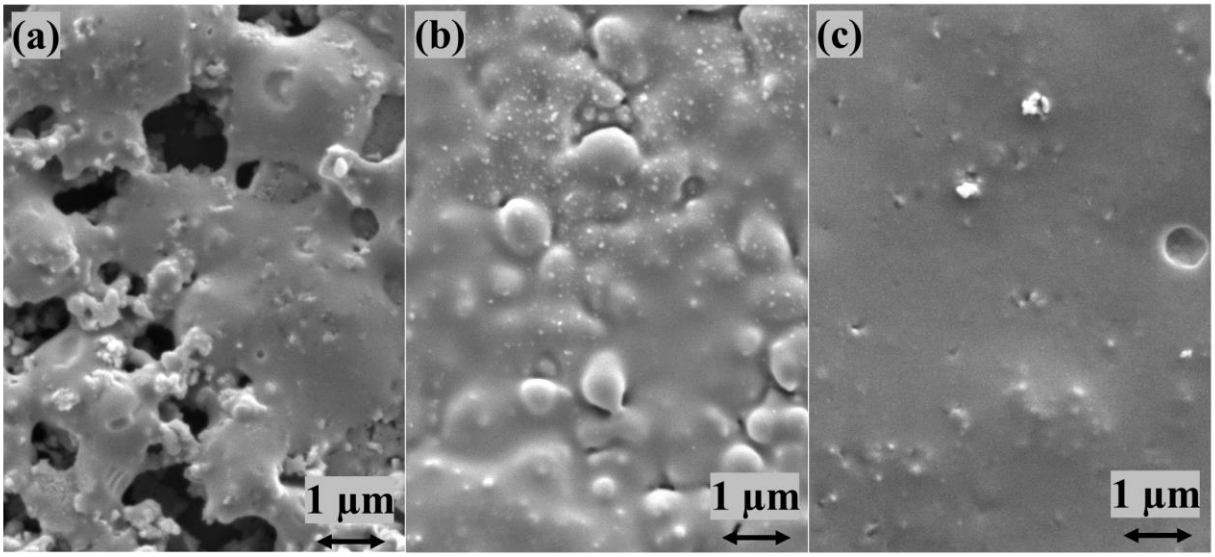

Figure 14. SEM images of surface morphology of IR 1070 nm laser-sintered GeSn films with 15% Sn ratio in the film (a) IR laser sintered at 20 W, (b) IR laser sintered at 25 W, (c) IR 1070 laser sintered at 30 W.

4.2.4. GeSn film cross-sections

The SEM cross-sectional images of as-deposited and IR laser-sintered GeSn films are shown in figure 15. Figure 15(a) shows as-deposited GeSn films, where particles are interconnected to form the film, but it has large surface voids and poor adhesion to the substrate. The thickness of the as-deposited

film is around 3 μm on top of a 2 μm SiO_2 insulating layer. Figure 15(b) shows the cross-section of IR laser sintered film at relatively moderate power, where particles mostly melted and formed a dense film with some noticeable non-wetting effect of Sn. If adequate power is used in IR laser sintering, then the films completely melt and form a more flattened surface, as shown in figure 15(c). The LS process lowered surface voids and reduced film thickness to 2 μm. The LS process also increased adhesion strength between the film and substrate.

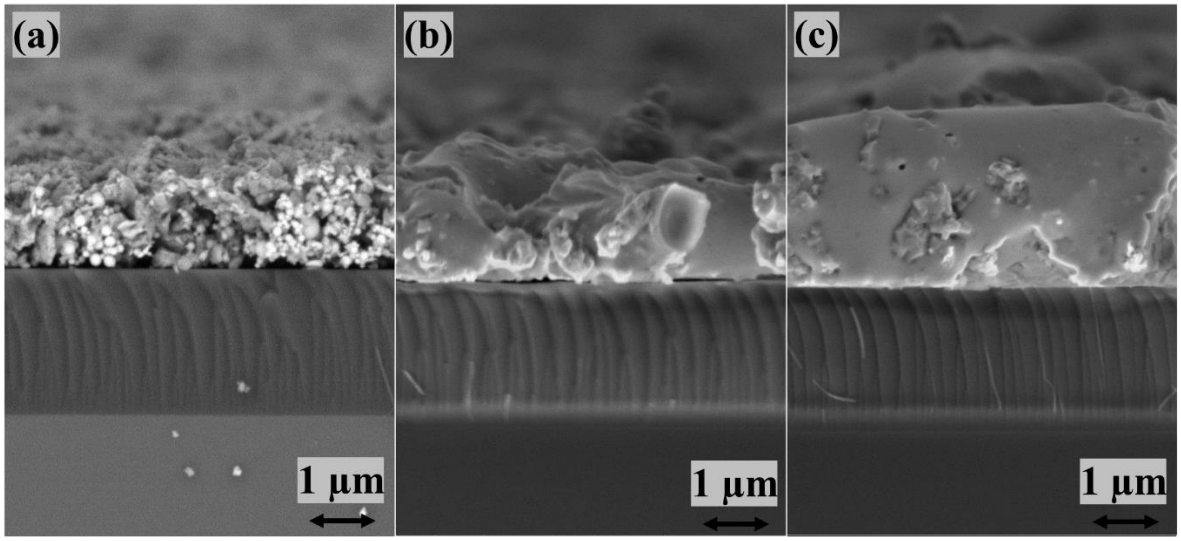

Figure 15. SEM cross-sectional images of as-deposited and IR laser-sintered GeSn films with different laser parameters. (a) as-deposited GeSn films, (b) IR 1070 laser-sintered at 25 W, and (c) IR 1070 laser-sintered at 30 W.

4.3. Elemental Composition

For elemental composition analysis, only IR 1070 nm laser-sintered samples were considered. The as-deposited GeSn film showed 32% Ge, 15% Sn, and 53% oxygen, found by EDX analysis. The IR laser sintered GeSn film showed approximately 40% Ge, 12% Sn, and 48% oxygen, as shown in figure 16 (f). The as-deposited film contains a high amount of oxygen due to the involved fabrication process. During the IR laser recrystallization process, the amount of oxygen is reduced from 53% to 48% due to oxygen removal from the top surface. Thus, the amount of Ge increased from 32% to 40% by breaking down some parts of the oxides (GeO_x). The reduction of oxygen may come from the film surface as the LS process starts melting and recrystallizing the films. Also, ablation occurs during the LS process,

which eventually causes some Sn loss from the films. The amount of tin is reduced from 15% to 12%. The elemental mapping also shows that all the elements (Ge, Sn, and O_2) are uniformly distributed throughout the film except the areas where the Sn balling effect is visible.

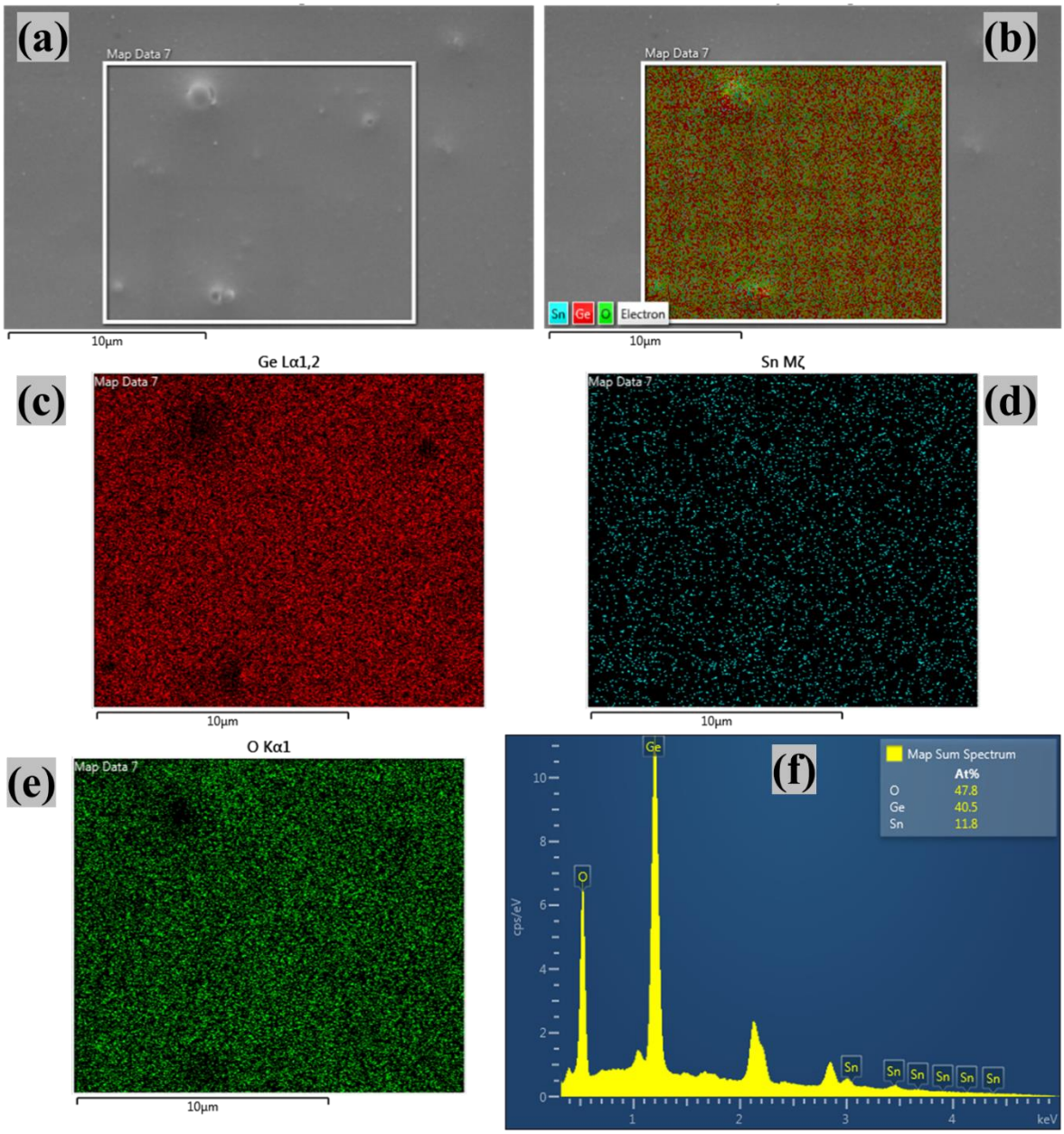

Figure 16. The typical EDX spectra (mapping) of the GeSn thin films with 12% Sn ratio, which is IR 1070 nm laser-sintered at 30 W. (a) and (b) elemental mapping analysis and distribution of each element, Ge in (c), Sn in (d), and O_2 in (e). EDX peak and the molecular weight ratio of all the elements are shown in (f).

4.4. Crystallinity Determination by Raman and XRD Measurements

Only IR 1070 nm laser sintered films were considered to better understand the physical impact of the LS process on the film properties.

4.4.1. Raman spectrum analysis

Raman spectrum for both as-deposited and laser-sintered films is shown in figure 17 for a 2% Sn ratio. The as-deposited Ge film showed a Ge-Ge vibrational mode peak around 298 cm^{-1}, as shown in figure 17 (green line). It shifted by 2 cm^{-1} from the standard crystalline Ge peak at 300 cm^{-1} due to the strain effect during ball milling of GeSn. The laser-sintered film with adequate power showed a sharp peak at 300 cm^{-1} with symmetrical distribution (at FWHM), as shown in figure 17 (red line). The FWHM is much smaller compared to the as-deposited GeSn film. It indicated that the laser-sintered GeSn film is completely crystallized and showed polycrystalline nature. Due to the very small amount of Sn, the Raman peaks still behave like Ge only. After laser sintering, the peak moved to 300 cm^{-1} with a long shoulder tail with small peaks indicating Sn contents in the film. These small peaks can be increased by adding more Sn in the film.

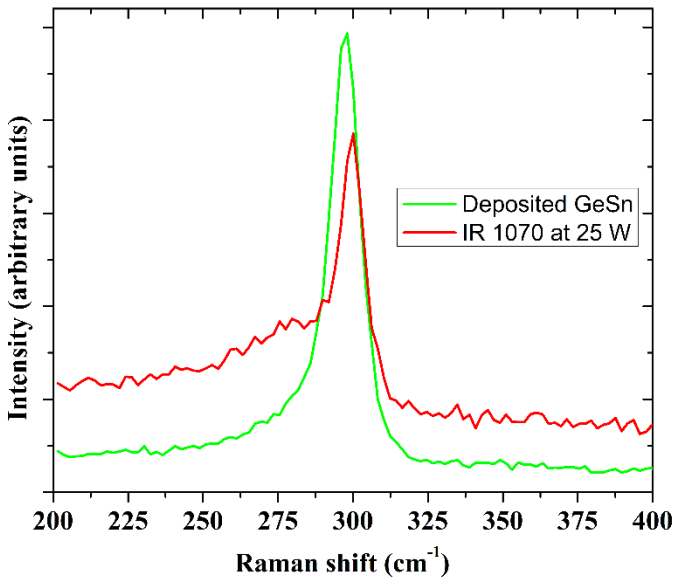

Figure 17. Raman spectra for the as-deposited and IR laser-sintered GeSn thin films with 2% Sn ratio, measured using a 514 nm laser excitation at room temperature.

Raman spectrum for as-deposited GeSn films with a 15% Sn ratio is shown in figure 18. H. Mahmodi et al. [67] indicated that the amount of Sn greatly controls the Ge-Ge vibrational peak position, which is usually shifted below 300 cm^{-1}. The as-deposited film with 15% Sn shows a major peak at 295.70 cm^{-1}, which is around 4.5 cm^{-1} left shift due to high Sn content. The Raman spectrum was measured for an area of 0.5x0.5 cm^2 mapping, which is shown in figure 18 (left). The average spectrum data is shown in figure 18 (right). The area mapping was considered for Raman spectrum analysis to get an overall idea of the film. V. R. D'Costa et al. [68] showed Sn-Sn vibrational mode around 175 cm^{-1}. We also noticed the Sn-Sn Raman peak at 175.9 cm^{-1}, as shown in figure 18.

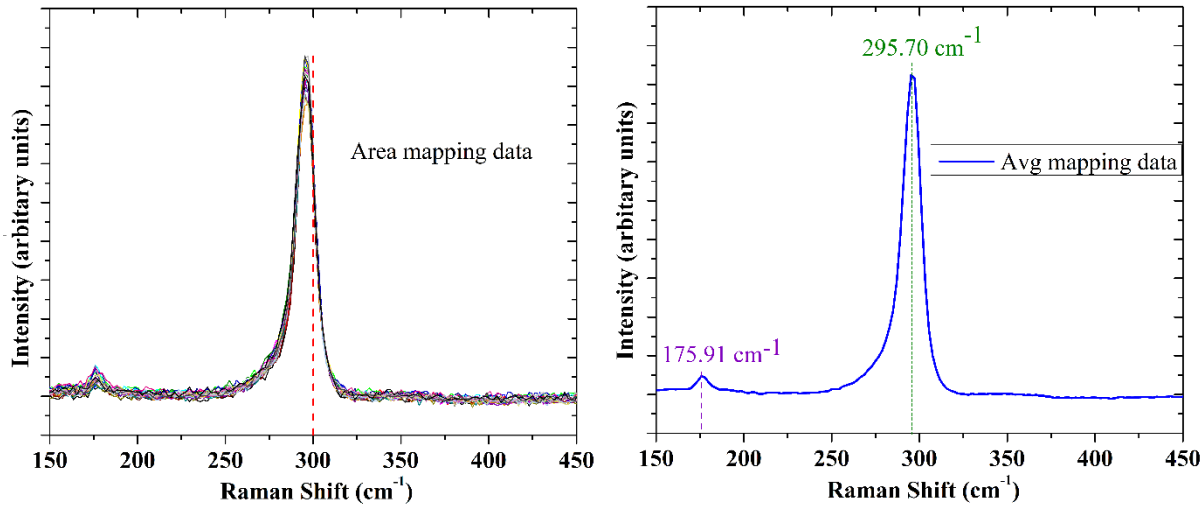

Figure 18. Raman spectra for the as-deposited GeSn thin films with a 15% Sn ratio, measured using a 514 nm laser excitation at room temperature. (left) area mapping Raman spectrum and (right) avg data of area mapping.

Raman spectrum for IR laser-sintered GeSn films with a 12% Sn ratio is shown in figure 19. The laser-sintered film with 12% Sn shows a major peak at 295 cm^{-1}, which is around 5 cm^{-1} left shift due to the high Sn ratio. The Raman spectrum was measured for an area of 0.5x0.5 cm^2 mapping, which is shown in figure 19 (left). The average spectrum data is shown in figure 19 (right). The area mapping Raman spectrum would demonstrate the overall structure of the film. After sintering, the Sn-Sn vibrational mode is barely noticed due to more GeSn alloy formation. A high Sn ratio causes a long tail with a slow falling slope, which is visible in the sintered Raman spectrum between 250 cm^{-1} to 280 cm^{-1} [69], as shown in figure 19(b). There are some very small peaks in the 250 cm^{-1} to 280 cm^{-1} range, as

noticeable in the mapping data, figure 19(a). However, we used a 514 nm laser excitation for Raman spectroscopy, and it is very difficult to identify clear peaks with this excitation, which is below the resonance condition [67]. Probably a wavelength of 633 nm or 647.1 nm would be a good choice for Raman analysis [67].

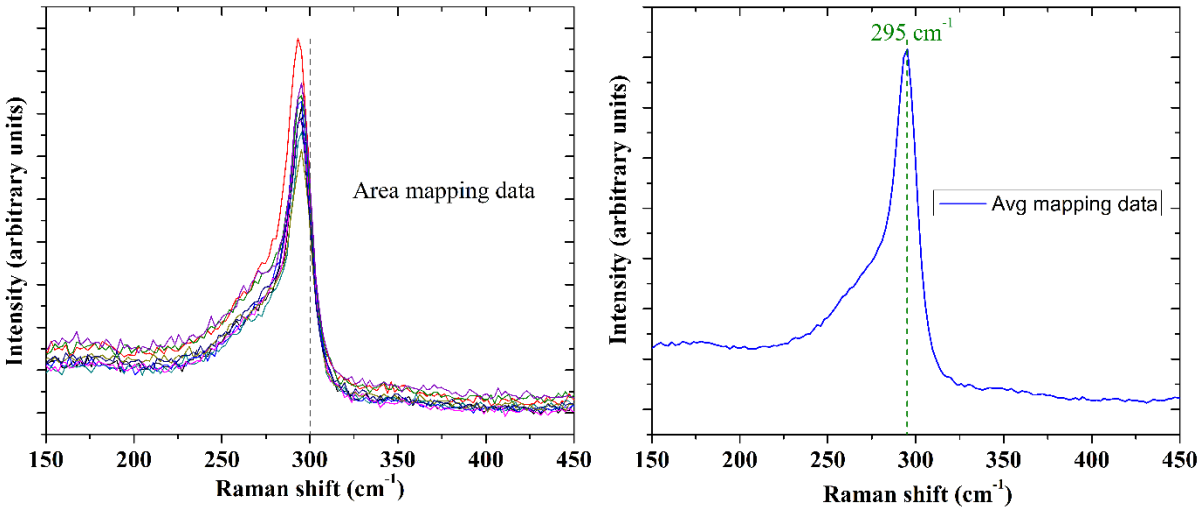

Figure 19. Raman spectra for the laser-sintered GeSn thin films with a 12% Sn ratio, measured using a 514 nm laser excitation at room temperature. (left) area mapping Raman spectrum and (right) avg data of area mapping.

4.4.2. XRD peak analysis

The XRD patterns for both as-deposited and IR laser-sintered GeSn films are shown in figure 20. Films after laser crystallization demonstrated the shifted peak position due to the high Sn ratio in the film. The as-deposited film is shown in the black curve, and the laser-sintered film is shown in the blue curve. The red dotted lines are drawn for each different peak, found from the literature review. Two major peaks of germanium dioxide were identified at a 2θ angle of 20.65° for GeO_2 (100) and 26.15° for GeO_2 (101), which are in alignment with the literature [56], [57]. The tin oxide peak was identified at a 2θ angle of 38.35° for SnO_2 (200) [47]. The XRD peaks of different Ge orientations were detected at a 2θ angle of 27.45° for Ge (111) [46], [47], [70], [71], 45.30° for Ge (220) [46], [47], [70], [71], 54.0° for Ge (311) [46], [47], [70], [71], and 66.30° for Ge (400) [69]–[72], which are similar to polycrystalline GeSn films reported in the literature. The XRD peaks of different Sn orientations were

found at a 2θ angle of 30.90° for Sn (200) [46], [70], [71], [73], 32.32° for Sn (101) [46], [70], [71], [73], 39.75° for Sn (220) [70], [71], 55.80° for Sn (301) [71], 63.0° for Sn (112) [70], [71], and 65.10° for Sn (321) [71]. As-deposited films show more individual peaks for Ge, Sn, and oxides of these two. The major peaks of Ge and Sn shifted after the LS process, and some of them showed a clear peak of GeSn. Shifted peaks are marked by green ovals, as shown in the laser-sintered sample.

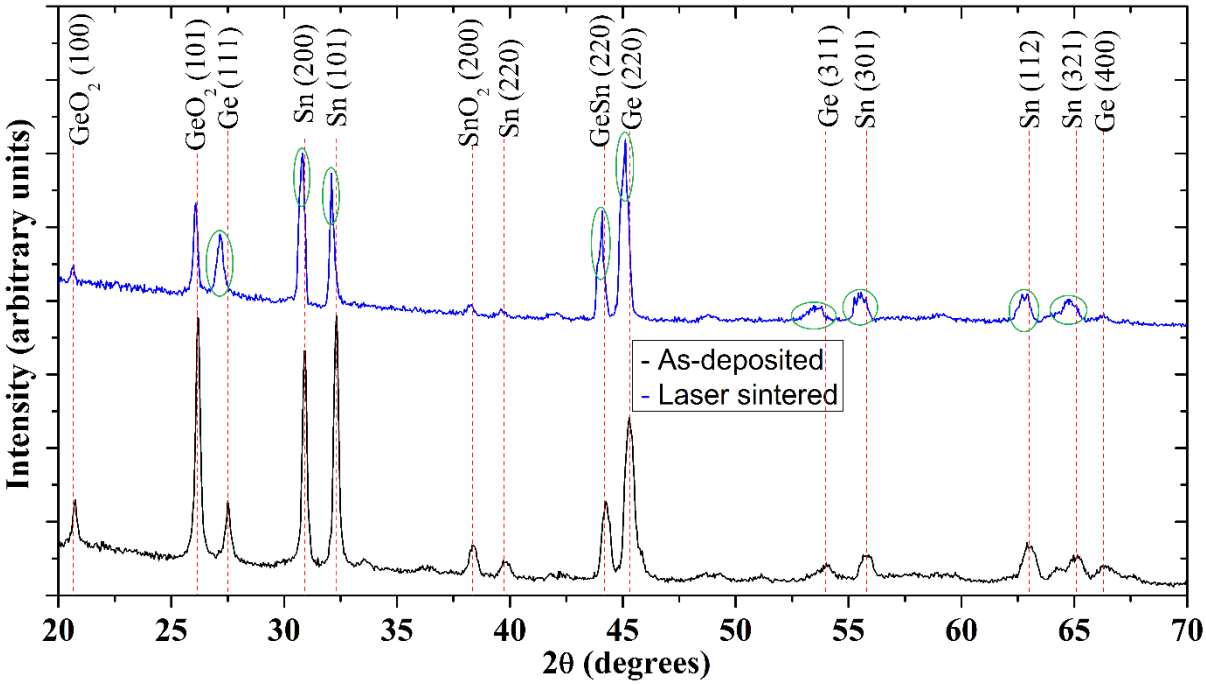

Figure 20. XRD peaks of as-deposited and IR laser-sintered GeSn thin films. The as-deposited film is shown at the bottom (black), and IR laser sintered film is shown at the top (blue).

M. Kim et al. [47] and N. Uchida et al. [74] showed that the GeSn (111) peak should be within 27.06° - 27.17°, and we found GeSn (111) peak at 27.15°. According to literature, GeSn (220) peak could be between 44.0° - 45.20° [46], [47], [70], [73], [74] and we found GeSn (111) peak at 44.20°. GeSn peaks are visible as the LS process helps to create GeSn alloy. However, segregated Sn is also noticeable in both as-deposited and laser-sintered films, as shown by Sn (200) and Sn (101). The amount of segregated Sn is reduced after the LS process. Overall, the XRD peaks are clear evidence of GeSn mixtures with alloy formation. The segregated Sn could be removed by chemical etching, by using an HCl solution [46].

4.5. Electrical Properties

Integrated photonic circuits (IPCs) and optoelectronic devices such as IR photodetectors require high-carrier mobility semiconductor films on insulators. The carrier mobility of the semiconductor device depends on the grain size of the fabricated films. The hole mobility, carrier concentration, and resistivity of as-deposited GeSn film with a 15% Sn ratio were measured as 47.4 $cm^2/V.s$, $1.80x10^{13}$ cm^{-3}, and $4.27x10^6$ Ω-cm, respectively. The hole mobility, carrier concentration, and resistivity of IR laser-sintered GeSn film were measured as 240 $cm^2/V.s$, $1.05x10^{13}$ cm^{-3}, and $1.94x10^5$ Ω-cm, respectively. The hole mobility of the laser-sintered GeSn film increased by five times compared to as-deposited films. Also, the mobility of GeSn film is higher than the Ge film. This clearly indicates the mobility enhancement by incorporating Sn in the film. Also, the LS process has a positive impact on improving the mobility of the film through crystallization. Additionally, the resistivity of the film decreased by order of magnitude due to the solidification of the film after melting by the LS process.

4.6. Optical Properties

The optical transmittance and reflectance spectra from 900 to 3000 nm of wavelength are shown in figure 21 for laser-sintered GeSn thin films. At room temperature, Ge is an indirect-bandgap material of 0.644 eV at the L point and a direct bandgap of 0.8 eV at the Γ point [75]. So, the absorption coefficient of Ge films drastically reduces above 1550 nm (equivalent to 0.8 eV) [75]–[77]. The absorption coefficient increases at wavelengths longer than 1550 nm with Sn incorporation in the film [75], [76]. The absorption coefficient also depends on the amount of Sn ratio in the film, the higher the Sn content higher the absorption coefficient [77]. So, the absorption enhancement in the IR region allows $Ge_{1-x}Sn_x$ devices to operate at a longer wavelength than Ge. The optical transmittance spectrum is shown in figure 21 (blue color), with no transmission below 1000 nm of wavelength due to the Si substrate. The transmittance of the fabricated GeSn thin film is around 15% in the near IR window and around 25% in the mid-IR window. Reported transmittance is very high using other fabrication methods, ranging from 25-50% for thin films [46], [78], [79]. We found low transmittance (15-25%) in the laser-sintered film.

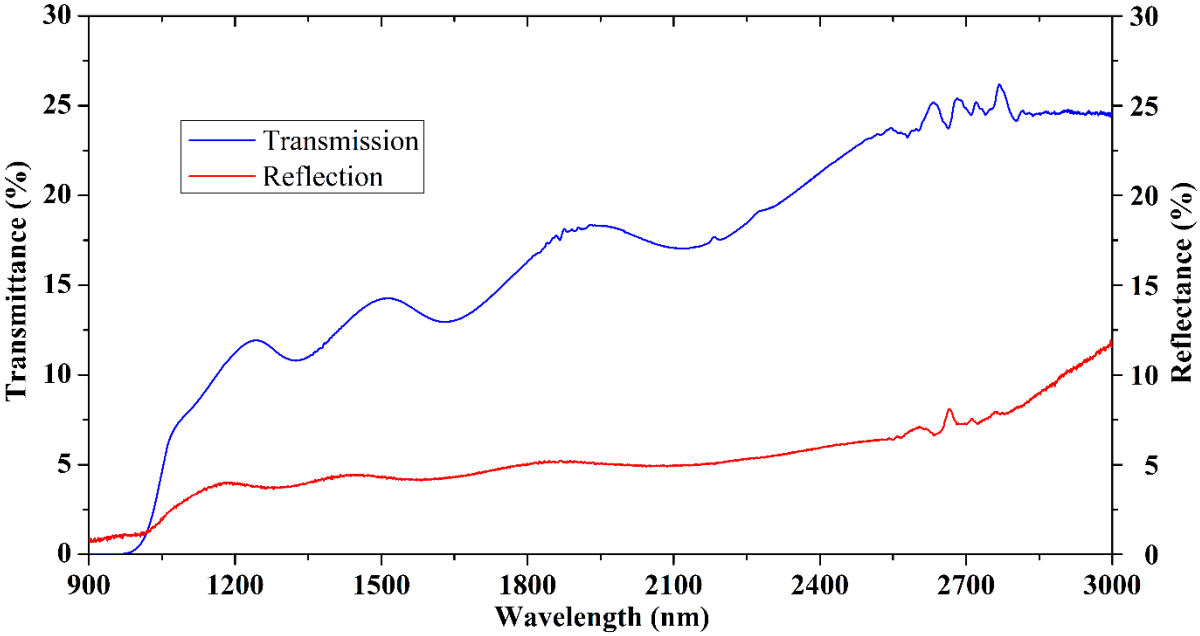

Figure 21. The optical transmittance spectra (blue line) and reflectance spectra (red line) of the laser-sintered polycrystalline GeSn thin film with 12% Sn.

The optical reflectance spectrum of the laser-sintered GeSn film is shown in figure 21 (red color). We found around 1% reflection loss in the visible wavelength regime, around 5% reflection loss in the near-IR wavelength regime, and around 10% reflection loss in the mid-IR wavelength regime. Other fabrication methods reported a comparatively high amount of reflection loss ranging from 10-20% [76], [77]. Scattering loss was also measured by using the Labsphere integrating sphere at a visible wavelength of 633 nm. The total scattering and reflection loss was found around 10% in the near-IR wavelength regime and around 15% in the mid-IR wavelength regime. So, the GeSn thin film significantly absorbs the IR light, including some loss due to reflectance and scattering. Also, the absorption of IR light may be hampered a little bit due to the unwanted oxygen in the film. It can be concluded that the laser-sintered film absorbs almost 70% of the light in the near to mid-IR regime with considering all the losses. Increasing IR light absorption from near to mid-IR is very effective in infrared imaging applications. It can be concluded from the measured optical spectrum that the laser-sintered polycrystalline GeSn thin films can be used for possibly mid-IR photodetection purposes.

4.7. Discussion

The LS process is very effective for simultaneous sintering and crystallization of the GeSn thin films. In the as-deposited GeSn films, both Ge and Sn microparticles are uniformly distributed throughout the surface. However, these particles are connected by very weak “Van der Waals” forces with lots of air gaps between NPs. The LS process can remove the surface porosity and air gaps between NPs as it melts and solidify the film. A dense and compact polycrystalline GeSn films were achieved after the LS process. Initially, GeSn films were fabricated using only a 2% Sn atomic ratio, then eventually moved to a 15% Sn ratio to get direct bandgap GeSn film.

Both UV and IR lasers were experimented with separately to fabricate polycrystalline GeSn thin films. We found that the IR laser in continuous mode is appropriate for sintering and recrystallizing the GeSn NPs. When sintering using the short pulse UV laser, the melted films do not get enough time to flow uniformly due to the non-wetting nature of Sn material. We still obtained a uniform melting and solidification by UV laser if the atomic Sn ratio is less than 5% in the GeSn film. However, the non-wetting behavior of Sn becomes very strong with a higher percentage of Sn ratio. So, the short pulse UV laser was not found suitable for GeSn films with 5% or more Sn in the film. Additionally, GeSn becomes a direct bandgap with an 8% or more Sn ratio in the film. So, we targeted for more than 10% Sn and achieved a smooth surface film with no air gaps in the GeSn film. Eventually, we solved this non-wetting issue of Sn using a continuous mode long pulse IR laser. The melted NPs get enough time to uniformly flow and solidify when sintering by IR 1070 nm long pulse laser. The results are shown in the SEM images.

The amount of oxygen in the film is decreased due to oxygen removal from the film surface during the LS process. However, all the oxygens cannot be removed from the inside of the film due to the rapid melting and solidification. Thus, some oxides (GeO_2 and SnO_2) were found in the films. Further film processing can be done to remove oxides from the film, especially using the furnace annealing method. J. Zhao et al. [80] recently did a furnace annealing study in an H_2 environment and showed a full conversion from GeO_2 to Ge at 700 °C.

In both as-deposited and laser-sintered films, the Ge-Ge vibrational mode Raman peak is shifted by 4-5 cm^{-1} from standard 300 cm^{-1} due to high Sn concentration in the film. Additionally, long-tail between 250-280 cm^{-1} with a very small peak is a clear indication of GeSn alloying in the film. The XRD analysis shows the oxidation (GeO_2 and SnO_2) and segregation of Sn in the films. However, the peak intensity of oxides and Sn becomes smaller after the LS process. The individual peak of Ge and Sn also shifted due to the GeSn mixture, which is shown in XRD with green ovals. The GeSn alloy peaks are also noticeable in the XRD analysis. Moreover, the GeSn thin film optical absorption is increased after the LS process as the surface reflection is reduced to 5-10%. The film transmittance was about 15-25%. Thus, the expected IR light absorption is around 70%. So, the LS process is very effective in melting, and recrystallizing the GeSn film. Furthermore, the mobility of the laser-sintered film is increased by almost six times compared to the as-deposited film due to the dense film after the LS process.

Chapter 5. Conclusion and Future Work

5.1. Conclusion

This work shows that the uniform Ge and GeSn thin film deposition can be achieved using a centrifugal force and subsequent LS process. At first, Ge films were deposited using Ge NCs solution in methanol produced from Ge NPs by ball milling and ultrasonication. Secondly, GeSn thin films were deposited using Ge and Sn NCs mixture solution in methanol produced from Ge and Sn NPs by ball milling and ultrasonication. The ratio of Ge and Sn was controlled by carefully weighing the particles for a fixed atomic ratio. The GeSn thin films were deposited in two phases. In the first phase, GeSn films were deposited with only 2% Sn concentration. In the second phase, the atomic Sn ratio was increased from 2% to 15% targeting direct bandgap GeSn thin films.

Effective utilization of both CW mode and pulse laser is demonstrated to simultaneously melt the NPs and recrystallize the film. We demonstrated that both pulse mode UV laser and CW mode IR laser can be used to melt and crystallize the Ge thin films. However, for the GeSn material, the laser conditions are different depending on the ratio of the Sn in the GeSn material system. For 2% Sn in the film, GeSn NPs can be melted and crystallized by using both UV and IR lasers. Still, UV laser causes some surface voids in the film due to the non-wetting nature of the Sn material. This non-wetting problem of Sn becomes so strong with a higher Sn ratio that the UV laser can no longer be used due to the short pulse duration. GeSn NPs don't get enough time to flow after melting. To overcome this issue, a long pulse IR laser in continuous mode is used and eventually proved very effective for both 2% and 15% Sn ratio in the film. Thus, the LS process is proven to fabricate dense semiconductor films by removing the surface porosity and film voids. It also provides strong adhesion of the film with the substrate. The LS process is a unique method to directly melt the NPs and form a smooth film on various substrates. The laser parameters can be controlled and optimized to melt different types of materials with their respective melting temperature.

The measured electrical and optical characteristics indicate that high-quality polycrystalline thin films can be obtained, which are appropriate for photonic devices, including IR photodetectors. The polycrystalline Ge thin films with a high hole mobility of 203 $cm^2/V.s$ were achieved through the LS

method. The mobility was increased to 240 $cm^2/V.s$ by 12% Sn incorporation in the film. However, the remaining oxygen in the films due to the fabrication process limitation hinders the performance of the films. The LS process can provide thick Ge and GeSn films over a large area with good hole mobility values. The IR laser proved more effective in melting the thin films compared to the UV laser. We successfully deposited both Ge and GeSn thin films from microparticles and solidified the film by using the LS process. The LS process is shown to directly melt Ge and Sn particles to fabricate the films. The fabricated films can be applied for near and mid-IR photodetection. The laser-assisted fabrication is used to eliminate the furnace annealing step, which is a time-consuming process. The developed method also can be applied to other material systems as well. The laser parameters need to be optimized for other materials depending on their physical properties, including the melting temperature.

5.2. Future Work

We successfully fabricated both Ge and GeSn films by directly melting the nanoparticles by using the LS process. However, we have identified a significant amount of oxygen in both films. One of our focuses was to fabricate GeSn films with high hole mobility and the second focus was to demonstrate direct bandgap GeSn films for optoelectronic devices. The fabrication process needs to be controlled to avoid oxygen inclusion in the films. Thus, the performance of the film can be improved further. However, we have achieved GeSn thin films with high mobility and relatively higher electrical resistivity. After fabricating quality GeSn thin films, pattering for device development is necessary to use as photodetectors. Interestingly, laser processing can be used for selective patterning towards complete device fabrication. The size of the developed films was 1x2 cm^2. Another challenge would be developing large-area films. The laser parameters also need to be optimized for sintering large area thin films to fabricate focal plane array (FPA) devices. The LS process is also compatible with CMOS technology, as substrate heating is minimal, a key requirement for commercial deployment.

References

[1] C. Korkut, K. Çınar, İ. Kabaçelik, R. Turan, M. Kulakcı, and A. Bek, "Laser Crystallization of Amorphous Ge Thin Films via a Nanosecond Pulsed Infrared Laser," *Crystal Growth & Design*, vol. 21, no. 8, pp. 4632–4639, Jul. 2021, DOI: 10.1021/acs.cgd.1c00470.

[2] S. Su *et al.*, "GeSn p-i-n photodetector for all telecommunication bands detection," *Optics Express*, vol. 19, no. 7, pp. 6400–6405, Mar. 2011, DOI: 10.1364/oe.19.006400.

[3] K. Toko, R. Yoshimine, K. Moto, and T. Suemasu, "High-hole mobility polycrystalline Ge on an insulator formed by controlling precursor atomic density for solid-phase crystallization," *Scientific Reports*, vol. 7, no. 1, p. 16981, Dec. 2017, DOI: 10.1038/s41598-017-17273-6.

[4] S. Vadavalli *et al.*, "Optical properties of germanium nanoparticles synthesized by pulsed laser ablation in acetone," *Frontiers in Physics*, vol. 2, pp. 1–9, 2014, DOI: 10.3389/fphy.2014.00057.

[5] R. Matsumura and N. Fukata, "Self-organized 〈1 0 0〉 direction growth of germanium film on insulator obtained by high speed continuous wave laser annealing," *Materials Letters*, vol. 288, p. 129328, Apr. 2021, DOI: 10.1016/j.matlet.2021.129328.

[6] H. Watakabe, T. Sameshima, H. Kanno, and M. Miyao, "Electrical properties for poly-Ge films fabricated by pulsed laser annealing," *Thin Solid Films*, vol. 508, no. 1–2, pp. 315–317, Jun. 2006, DOI: 10.1016/j.tsf.2005.08.393.

[7] M. Oehme *et al.*, "GeSn-on-Si normal incidence photodetectors with bandwidths more than 40 GHz," *Optics Express*, vol. 22, no. 1, pp. 839–846, Jan. 2014, DOI: 10.1364/oe.22.000839.

[8] M. C. Gupta, J. T. Harrison, and M. T. Islam, "Photoconductive PbSe thin films for infrared imaging," *Materials Advances*, vol. 2, no. 10. Royal Society of Chemistry, pp. 3133–3160, May 21, 2021. DOI: 10.1039/d0ma00965b.

[9] K. Kumari, S. Vura, S. Raghavan, and S. Avasthi, "Wafer scale epitaxial germanium on silicon (0 0 1) using pulsed laser annealing," *Materials Letters*, vol. 285, p. 129208, Feb. 2021, DOI: 10.1016/j.matlet.2020.129208.

[10] B. Rashmi Rao, N. Bhat, and S. K. Sikdar, "Thick PECVD Germanium Films for MEMS Application," in *Environmental Science and Engineering book series (ESE)*, 2014, pp. 469–471. DOI: 10.1007/978-3-319-03002-9_117.

[11] G. M. Beensh-Marchwicka, W. Mielcarek, and E. Prociów, "Evaluation of pulse magnetron sputtered Ge films doped with antimony for sensors application," in *Sensors and Actuators, B: Chemical*, Jun. 2001, vol. 76, pp. 361–365. DOI: 10.1016/S0925-4005(01)00633-5.

[12] D. M. A. MacKenzie and S. A. Brown, "Germanium nano-cluster films as humidity and hydrogen sensors," *Journal of Applied Physics*, vol. 112, no. 7, Oct. 2012, DOI: 10.1063/1.4758284.

[13] D. Marris-Morini *et al.*, "Germanium-based integrated photonics from near- to mid-infrared applications," *Nanophotonics*, vol. 7, no. 11. De Gruyter, pp. 1781–1793, Nov. 01, 2018. DOI: 10.1515/nanoph-2018-0113.

[14] Y. Ishikawa and K. Wada, "Germanium for silicon photonics," *Thin Solid Films*, vol. 518, no. 6 SUPPL. 1, Jan. 2010, DOI: 10.1016/j.tsf.2009.10.062.

[15] S. J. Koester, J. D. Schaub, G. Dehlinger, and J. O. Chu, “Germanium-on-SOI infrared detectors for integrated photonic applications,” *IEEE Journal on Selected Topics in Quantum Electronics*, vol. 12, no. 6, pp. 1489–1502, 2006, DOI: 10.1109/JSTQE.2006.883160.

[16] G. Z. Mashanovich *et al.*, “Germanium Mid-Infrared Photonic Devices,” *Journal of Lightwave Technology*, vol. 35, no. 4, pp. 624–630, Feb. 2017, DOI: 10.1109/JLT.2016.2632301.

[17] V. Reboud *et al.*, “Germanium based photonic components toward a full silicon/germanium photonic platform,” *Progress in Crystal Growth and Characterization of Materials*, vol. 63, no. 2, pp. 1–24, Jun. 2017, DOI: 10.1016/j.pcrysgrow.2017.04.004.

[18] P. Vines *et al.*, “High performance planar germanium-on-silicon single-photon avalanche diode detectors,” *Nature Communications*, vol. 10, no. 1, Dec. 2019, DOI: 10.1038/s41467-019-08830-w.

[19] R. E. Warburton *et al.*, “Ge-on-si single-photon avalanche diode detectors: Design, modeling, fabrication, and characterization at wavelengths 1310 and 1550 nm,” *IEEE Transactions on Electron Devices*, vol. 60, no. 11, pp. 3807–3813, 2013, DOI: 10.1109/TED.2013.2282712.

[20] L. F. Llin *et al.*, “High sensitivity Ge-on-Si single-photon avalanche diode detectors,” *Optics Letters*, vol. 45, no. 23, p. 6406, Dec. 2020, DOI: 10.1364/ol.396756.

[21] K. Toko, I. Nakao, T. Sadoh, T. Noguchi, and M. Miyao, “Electrical properties of poly-Ge on glass substrate grown by two-step solid-phase crystallization,” *Solid-State Electronics*, vol. 53, no. 11, pp. 1159–1164, Jun. 2009, DOI: 10.1016/j.sse.2009.08.002.

[22] H. W. Jung, W. S. Jung, H. Y. Yu, and J. H. Park, “Electrical properties of phosphorus-doped polycrystalline germanium formed by solid-phase and metal-induced crystallization,” *Journal of Alloys and Compounds*, vol. 561. Elsevier Ltd, pp. 231–233, Jun. 05, 2013. DOI: 10.1016/j.jallcom.2013.02.023.

[23] K. Toko, R. Numata, N. Oya, N. Fukata, N. Usami, and T. Suemasu, “Low-temperature (180 °C) formation of large-grained Ge (111) thin film on insulator using accelerated metal-induced crystallization,” *Applied Physics Letters*, vol. 104, no. 2, p. 022106, Jan. 2014, DOI: 10.1063/1.4861890.

[24] S. Hu, A. F. Marshall, and P. C. McIntyre, “Interface-controlled layer exchange in metal-induced crystallization of germanium thin films,” *Applied Physics Letters*, vol. 97, no. 8, p. 082104, Aug. 2010, DOI: 10.1063/1.3480600.

[25] M. Tada *et al.*, “Low Temperature Germanium Growth on Silicon Oxide Using Boron Seed Layer and In Situ Dopant Activation,” *Journal of The Electrochemical Society*, vol. 157, no. 3, p. H371, 2010, DOI: 10.1149/1.3295703.

[26] J. T. Harrison, E. Pantoja, M. H. Jang, and M. C. Gupta, “Laser sintered PbSe semiconductor thin films for Mid-IR applications using nanocrystals,” *Journal of Alloys and Compounds*, vol. 849, Dec. 2020, DOI: 10.1016/j.jallcom.2020.156537.

[27] A. Sinha, A. Soman, U. Das, S. Hegedus, and M. C. Gupta, “Nanosecond Pulsed Laser Patterning of Interdigitated Back Contact Heterojunction Silicon Solar Cells,” *IEEE Journal of Photovoltaics*, vol. 10, no. 6, pp. 1648–1656, Nov. 2020, DOI: 10.1109/JPHOTOV.2020.3026907.

[28] O. R. Musaev, E. A. Sutter, J. M. Wrobel, and M. B. Kruger, “Au, Ge, and AuGe nanoparticles fabricated by laser ablation,” *Journal of Nanoparticle Research*, vol. 14, no. 2, p. 654, Feb. 2012, DOI: 10.1007/s11051-011-0654-y.

[29] S. Wirths, D. Buca, and S. Mantl, “Si-Ge-Sn alloys: From growth to applications,” *Progress in Crystal Growth and Characterization of Materials*, vol. 62, no. 1. pp. 1–32, 2016. DOI: 10.1016/j.pcrysgrow.2015.11.001.

[30] T. T. Tran *et al.*, “Synthesis of Ge1-xSnx alloys by ion implantation and pulsed laser melting: Towards a group IV direct bandgap material,” *Journal of Applied Physics*, vol. 119, no. 18, p. 183102, May 2016, DOI: 10.1063/1.4948960.

[31] P. Ščajev *et al.*, “Extension of spectral sensitivity of GeSn IR photodiode after laser annealing,” *Applied Surface Science*, vol. 555, p. 149711, Jul. 2021, DOI: 10.1016/j.apsusc.2021.149711.

[32] N. Uchida *et al.*, “Carrier and heat transport properties of poly-crystalline GeSn films for thin-film transistor applications,” *Journal of Applied Physics*, vol. 126, no. 14, p. 145105, Oct. 2019, DOI: 10.1063/1.5085470.

[33] T. Maeda *et al.*, “Ultrathin GeSn p-channel MOSFETs grown directly on Si(111) substrate using solid phase epitaxy,” in *Japanese Journal of Applied Physics*, 2015, vol. 54, no. 4, p. 04DA07. DOI: 10.7567/JJAP.54.04DA07.

[34] S. Wirths *et al.*, “Lasing in direct-bandgap GeSn alloy grown on Si,” *Nature Photonics*, vol. 9, no. 2, pp. 88–92, 2015, DOI: 10.1038/nphoton.2014.321.

[35] D. Stange *et al.*, “GeSn/SiGeSn Heterostructure and Multi Quantum Well Lasers,” *ACS Photonics*, vol. 5, no. 11, pp. 4628–4636, 2018, DOI: 10.1021/acsphotonics.8b01116.

[36] T. N. Pham *et al.*, “Si-based Ge0.9Sn0.1 photodetector with peak responsivity of 2.85 A/W and longwave cutoff at 2.4 μm,” *Electronics Letters*, vol. 51, no. 11, pp. 854–856, May 2015, DOI: 10.1049/el.2015.0331.

[37] S. Al-Kabi *et al.*, “Study of High-Quality GeSn Alloys Grown by Chemical Vapor Deposition towards Mid-Infrared Applications,” *Journal of Electronic Materials*, vol. 45, no. 12, pp. 6251–6257, Dec. 2016, DOI: 10.1007/s11664-016-5028-x.

[38] M. Oehme *et al.*, “GeSn p-i-n detectors integrated on Si with up to 4% Sn,” *Applied Physics Letters*, vol. 101, no. 14, 2012, DOI: 10.1063/1.4757124.

[39] K. Moto, R. Matsumura, T. Sadoh, H. Ikenoue, and M. Miyao, “Pulse number controlled laser annealing for GeSn on insulator structure with high substitutional Sn concentration,” *Applied Physics Letters*, vol. 108, no. 26, Jun. 2016, DOI: 10.1063/1.4955059.

[40] S. Stefanov *et al.*, “Laser synthesis of germanium tin alloys on virtual germanium,” *Applied Physics Letters*, vol. 100, no. 10, Mar. 2012, DOI: 10.1063/1.3692175.

[41] M. Kurosawa, N. Taoka, H. Ikenoue, O. Nakatsuka, and S. Zaima, “Large grain growth of Ge-rich Ge1-xSnx (x 0.02) on insulating surfaces using pulsed laser annealing in flowing water,” *Applied Physics Letters*, vol. 104, no. 6, Oct. 2014, DOI: 10.1063/1.4864627.

[42] S. Oguz, W. Paul, T. F. Deutsch, B. Y. Tsaur, and D. V. Murphy, “Synthesis of metastable, semiconducting Ge-Sn alloys by pulsed UV laser crystallization,” *Applied Physics Letters*, vol. 43, no. 9, pp. 848–850, 1983, DOI: 10.1063/1.94524.

[43] B. R. Conley *et al.*, “Si based GeSn photoconductors with a 1.63 A/W peak responsivity and a 2.4 μ m long-wavelength cutoff,” *Applied Physics Letters*, vol. 105, no. 22, Dec. 2014, DOI: 10.1063/1.4903540.

[44] J. Xie *et al.*, “Molecular approaches to p- and n-nanoscale doping of Ge1-ySny semiconductors: Structural, electrical and transport properties,” *Solid-State Electronics*, vol. 53, no. 8, pp. 816–823, Aug. 2009, DOI: 10.1016/j.sse.2009.04.013.

[45] R. R. Lieten *et al.*, “Tensile strained GeSn on Si by solid phase epitaxy and fabrication of high mobility FET devices,” in *Solid State Devices and Materials*, Sep. 2013, pp. 1202–1203. DOI: 10.7567/ssdm.2013.p-2-3.

[46] H. Li, J. Brouillet, A. Salas, X. Wang, and J. Liu, “Low temperature growth of high crystallinity GeSn on amorphous layers for advanced optoelectronics,” *Optical Materials Express*, vol. 3, no. 9, pp. 1385–1396, Sep. 2013, DOI: 10.1364/ome.3.001385.

[47] M. Kim *et al.*, “Polycrystalline GeSn thin films on Si formed by alloy evaporation,” *Applied Physics Express*, vol. 8, no. 6, Jun. 2015, DOI: 10.7567/APEX.8.061301.

[48] L. Zhang *et al.*, “Formation of high-Sn content polycrystalline GeSn films by pulsed laser annealing on co-sputtered amorphous GeSn on Ge substrate,” *Chinese Physics B*, vol. 26, no. 11, Nov. 2017, DOI: 10.1088/1674-1056/26/11/116802.

[49] K. Toko, N. Oya, N. Saitoh, N. Yoshizawa, and T. Suemasu, “70 °c synthesis of high-Sn content (25%) GeSn on insulator by Sn-induced crystallization of amorphous Ge,” *Applied Physics Letters*, vol. 106, no. 8, Feb. 2015, DOI: 10.1063/1.4913744.

[50] S. Stefanov *et al.*, “Laser assisted formation of binary and ternary Ge/Si/Sn alloys,” in *Thin Solid Films*, Feb. 2012, vol. 520, no. 8, pp. 3262–3265. DOI: 10.1016/j.tsf.2011.10.101.

[51] A. Belkind and S. Gershman, “Artigo de revista: Plasma cleaning of surfaces,” *Vacuum Technology & Coating*, 2008.

[52] W. W. Balwanz, “Plasma Cleaning of Surfaces,” in *Surface Contamination*, Springer US, 1979, pp. 255–269. DOI: 10.1007/978-1-4684-3506-1_17.

[53] R. Ahmed and M. C. Gupta, “Mid-infrared photoresponse of electrodeposited PbSe thin films by laser processing and sensitization,” *Optics and Lasers in Engineering*, vol. 134, Nov. 2020, DOI: 10.1016/j.optlaseng.2020.106299.

[54] A. R. Zanatta, “Temperature-dependent Raman scattering of the Ge + GeOx system and its potential as an optical thermometer,” *Results in Physics*, vol. 19, p. 103500, 2020, DOI: 10.1016/j.rinp.2020.103500.

[55] M. S. Z. Abidin, Shahjahan, and A. M. Hashim, “Synthesis of germanium dioxide microclusters on silicon substrate in non-aqueous solution by electrochemical deposition,” *Indonesian Journal of Electrical Engineering and Computer Science*, vol. 6, no. 1, pp. 193–199, 2017, DOI: 10.11591/ijeecs.v6.i1.pp193-199.

[56] H. Jia, R. Kloepsch, X. He, J. P. Badillo, M. Winter, and T. Placke, “One-step synthesis of novel mesoporous three-dimensional GeO2 and its lithium storage properties,” *Journal of Materials Chemistry A*, vol. 2, no. 41, pp. 17545–17550, Nov. 2014, DOI: 10.1039/c4ta03933e.

[57] P. K. Giri and S. Dhara, “Freestanding Ge/GeO2 core-shell nanocrystals with varying sizes and shell thicknesses: Microstructure and photoluminescence studies,” *Journal of Nanomaterials*, vol. 2012, 2012, DOI: 10.1155/2012/905178.

[58] T. Imajo, T. Suemasu, and K. Toko, “Strain effects on polycrystalline germanium thin films,” *Scientific Reports*, vol. 11, no. 1, p. 8333, 2021, DOI: 10.1038/s41598-021-87616-x.

[59] S. Peng, D. Hu, and D. He, “Low-temperature preparation of polycrystalline germanium thin films by Al-induced crystallization,” *Applied Surface Science*, vol. 258, no. 16, pp. 6003–6006, 2012, DOI: 10.1016/j.apsusc.2012.02.080.

[60] G. O. Park *et al.*, “Enhanced thermoelectric properties of germanium powder/poly(3,4-ethylenedioxythiophene):poly(4-styrenesulfonate) composites,” *Thin Solid Films*, vol. 566, pp. 14–18, 2014, DOI: 10.1016/j.tsf.2014.07.011.

[61] H. A. Kasirajan *et al.*, “Low-hole concentration polycrystalline germanium by CO2 laser annealing for the fabrication of an enhancement-mode nMOSFET,” *Applied Physics Express*, vol. 11, no. 10, p. 101305, Oct. 2018, DOI: 10.7567/APEX.11.101305.

[62] K. Usuda, Y. Kamata, Y. Kamimuta, T. Mori, M. Koike, and T. Tezuka, “High-performance poly-Ge short-channel metal-oxide-semiconductor field-effect transistors formed on SiO2 layer by flash lamp annealing,” *Applied Physics Express*, vol. 7, no. 5, p. 056501, 2014, DOI: 10.7567/APEX.7.056501.

[63] T. Sadoh, H. Kamizuru, A. Kenjo, and M. Miyao, “Low-temperature formation (<500 °c) of poly-Ge thin-film transistor with NiGe Schottky source/drain,” *Applied Physics Letters*, vol. 89, no. 19, p. 192114, 2006, DOI: 10.1063/1.2387136.

[64] C. Y. Tsao, J. W. Weber, P. Campbell, G. Conibeer, D. Song, and M. A. Green, “In situ low temperature growth of poly-crystalline germanium thin film on glass by RF magnetron sputtering,” in *Solar Energy Materials and Solar Cells*, Sep. 2010, vol. 94, no. 9, pp. 1501–1505. DOI: 10.1016/j.solmat.2010.02.035.

[65] A. A. Akl and H. Howari, “Nanocrystalline formation and optical properties of germanium thin films prepared by physical vapor deposition,” *Journal of Physics and Chemistry of Solids*, vol. 70, no. 10, pp. 1337–1343, Oct. 2009, DOI: 10.1016/j.jpcs.2009.07.016.

[66] W. J. H. Berghuis, J. Melskens, B. Macco, R. J. Theeuwes, M. A. Verheijen, and W. M. M. Kessels, “Surface passivation of germanium by atomic layer deposited Al2O3 nanolayers,” *Journal of Materials Research*, vol. 36, no. 3, pp. 571–581, Feb. 2021, doi: 10.1557/s43578-020-00052-x.

[67] H. Mahmodi, M. R. Hashim, and U. Hashim, “Formation of nanocrystalline GeSn thin film on Si substrate by sputtering and rapid thermal annealing,” *Superlattices and Microstructures*, vol. 98, pp. 235–241, Oct. 2016, DOI: 10.1016/j.spmi.2016.08.030.

[68] V. R. D’Costa, J. Tolle, R. Roucka, C. D. Poweleit, J. Kouvetakis, and J. Menéndez, “Raman scattering in Ge1-ySny alloys,” *Solid State Communications*, vol. 144, no. 5–6, pp. 240–244, Nov. 2007, DOI: 10.1016/j.ssc.2007.08.020.

[69] W. Du *et al.*, “Silicon-based Ge 0.89 Sn 0.11 photodetector and light emitter towards mid-infrared applications,” in *Silicon Photonics XII*, Feb. 2017, vol. 10108, p. 1010813. DOI: 10.1117/12.2253067.

[70] H. Khelidj *et al.*, “Ge(Sn) growth on Si(001) by magnetron sputtering,” *Materials Today Communications*, vol. 26, Mar. 2021, DOI: 10.1016/j.mtcomm.2020.101915.

[71] Y. J. Cho *et al.*, “Germanium-tin alloy nanocrystals for high-performance lithium ion batteries,” *Physical Chemistry Chemical Physics*, vol. 15, no. 28, pp. 11691–11695, Jul. 2013, DOI: 10.1039/c3cp51366a.

[72] J. Zheng *et al.*, “Growth of high-Sn content (28%) GeSn alloy films by sputtering epitaxy,” *Journal of Crystal Growth*, vol. 492, pp. 29–34, Jun. 2018, DOI: 10.1016/j.jcrysgro.2018.04.008.

[73] L. Jin *et al.*, “Large area Germanium Tin nanometer optical film coatings on highly flexible aluminum substrates,” *Scientific Reports*, vol. 6, Sep. 2016, DOI: 10.1038/srep34030.

[74] N. Uchida *et al.*, “Carrier and heat transport properties of polycrystalline GeSn films on SiO2,” *Applied Physics Letters*, vol. 107, no. 23, Dec. 2015, DOI: 10.1063/1.4937386.

[75] A. Mosleh *et al.*, “Material characterization of Ge1-x Sn x alloys grown by a commercial CVD system for optoelectronic device applications,” *Journal of Electronic Materials*, vol. 43, no. 4, pp. 938–946, Apr. 2014, DOI: 10.1007/s11664-014-3089-2.

[76] K. Ye *et al.*, “Absorption coefficients of GeSn extracted from PIN photodetector response,” *Solid-State Electronics*, vol. 110, pp. 71–75, Aug. 2015, DOI: 10.1016/j.sse.2015.01.017.

[77] S. Bechler *et al.*, “Franz-Keldysh Effect in GeSn Detectors,” *ECS Transactions*, vol. 64, no. 6, pp. 383–390, Aug. 2014, DOI: 10.1149/06406.0383ecst.

[78] D. Zhang *et al.*, “MBE growth of ultra-thin GeSn film with high Sn content and its infrared/terahertz properties,” *Journal of Alloys and Compounds*, vol. 665, pp. 131–136, Apr. 2016, DOI: 10.1016/j.jallcom.2016.01.038.

[79] R. Ranjan, K. Barman, and M. K. Das, “Growth and characterization of GeSn alloys using RF sputtering,” in *2018 3rd International Conference on Microwave and Photonics, ICMAP 2018*, May 2018, vol. 2018-Janua, pp. 1–2. DOI: 10.1109/ICMAP.2018.8354636.

[80] J. Zhao, L. Yang, J. A. McLeod, and L. Liu, “Reduced GeO2 Nanoparticles: Electronic Structure of a Nominal GeOx Complex and Its Stability under H2 Annealing,” *Scientific Reports*, vol. 5, Dec. 2015, DOI: 10.1038/srep17779.

Appendix: List of Publications

1. M. T. Islam and M. C. Gupta, "Synthesis, structural, optical, and electrical properties of continuous wave and pulse laser sintered semiconductor Ge films," *Semicond. Sci. Technol.*, Nov. 2021. [*under review*]
2. M. T. Islam and M. C. Gupta, "Laser sintering of polycrystalline Ge-Sn films," in *Proceedings of IEEE 18th International Conference on Group IV Photonics (GFP).*, 7-10 Dec. 2021, Malaga, Spain. [*accepted*]
3. M. T. Islam and M. C. Gupta, "Polycrystalline GeSn thin films by simultaneous laser sintering and recrystallization," *Journal of Alloys and Compounds*, Dec. 2021. [*under review*].
4. M. C. Gupta, J. T. Harrison, and M. T. Islam, "Photoconductive PbSe thin films for infrared imaging," *Materials Advances*, vol. 2, no. 10. Royal Society of Chemistry, pp. 3133–3160, May 21, 2021 (published review article).

Synthesis, Structural, Optical, and Electrical Properties of Continuous Wave and Pulse Laser Sintered Semiconductor Ge Films

Md Toriqul Islam[1] and Mool C. Gupta[1]

[1]Department of Electrical and Computer Engineering, University of Virginia, Charlottesville, VA 22904, USA

Email: mgupta@virginia.edu

Abstract

The crystallization process of Ge films by a continuous wave (CW) and a pulsed laser is very effective for producing smooth, homogeneous, and crack-free polycrystalline films to use in transistors, photodetectors, and photovoltaic applications. However, little progress has been made to directly crystallize Ge films based on micro/nanoparticles (NPs) using the laser sintering (LS) process. In this paper, a simultaneous LS and crystallization process of Ge micro/nanoparticles to develop thick polycrystalline films on silicon substrates is demonstrated. Silicon substrates with a SiO_2 insulating layer on top were considered for compatibility with complementary metal-oxide-semiconductor (CMOS) technology. The LS process was applied to solution deposited micro/nanoparticles, 5 µm thick Ge films using both CW mode (infrared (IR) laser of wavelength 1070 nm) and pulse mode (UV laser of wavelength 355 nm) laser. After the LS process, around 2-2.5 µm thick film of polycrystalline Ge (pc-Ge) was achieved with optical and electrical properties comparable to traditionally developed chemical vapor deposited films. The crystallinity of the pc-Ge films was evaluated by Raman spectroscopy and XRD diffraction. The laser-sintered films exhibited a Raman peak at 300 cm^{-1} and XRD 2θ peak at 27.35, which indicated the poly-crystalline structure. The fabricated film showed high hole mobility of 203 $cm^2/V.s$, without any doping and film electrical resistivity value of $6.24x10^5$ Ω-cm. The developed LS process allows the quick deposition of polycrystalline thick films, removing surface porosity and voids, increasing films adhesion with the substrate, and faster thermal annealing.

Keywords: polycrystalline Ge, nanoparticle, laser sintering, crystallization, mobility, photodetector

Laser Sintering of Polycrystalline Ge-Sn Films

Md Toriqul Islam[1] and Mool C. Gupta[1]

[1]Department of Electrical and Computer Engineering, University of Virginia, Charlottesville, VA 22904, USA

Email: mgupta@virginia.edu

Abstract

A laser sintering fabrication process to deposit 3 μm thick GeSn films on silicon substrates has been demonstrated. A 2% tin was incorporated in germanium to increase p-type mobility. High hole mobility of 166.2 cm^2/v.s was achieved for laser-sintered polycrystalline GeSn films.

Keywords: polycrystalline, GeSn, laser sintering, mobility, infrared photodetector

Polycrystalline GeSn Thin Films by Simultaneous Laser Sintering and Recrystallization

Md Toriqul Islam[1] and Mool C. Gupta[1]

[1]Department of Electrical and Computer Engineering, University of Virginia, Charlottesville, VA 22904, USA

Email: mgupta@virginia.edu

Abstract

The near-infrared (IR) photodetection is usually achieved using InGaAs or Ge-based photodetectors. The detection range of Ge-based photodetectors can be expanded to the mid-IR using germanium-tin (GeSn) material systems due to its favorable physical characteristics. The GeSn thin film can be directly deposited on silicon substrates as it is fully compatible with silicon electronics. The laser sintering (LS) and crystallization process of GeSn thin films are very effective for creating smooth, homogeneous, and uniform polycrystalline films for electronic and photonic applications. There is not enough progress made to directly crystallize the GeSn thin films made of Ge and Sn nanoparticles (NPs) and the formation of alloy using the LS process. Here, we demonstrated a simultaneous LS and crystallization process of GeSn thin films prepared from solution-processed NPs. Silicon wafers with a thermally grown silicon dioxide (SiO_2) insulating layer on top were used for accurate electrical characterization of the film. The GeSn thin films were fabricated with two different Sn atomic percentages (2% and 15%). The thickness of solution deposited GeSn thin films of NPs was around 4-5 µm. The in-lab developed LS process was employed to the as-deposited thin film of GeSn using both continuous wave (CW) IR laser of wavelength 1070 nm and nanosecond pulsed ultraviolet (UV) laser of 355 nm wavelength. Around 2-2.5 µm thick polycrystalline GeSn films with 12% Sn were attained using the LS process. The fabricated films showed superior optical and electrical properties comparable to traditionally deposited films. The crystallinity of the polycrystalline GeSn thin films was assessed using both Raman spectroscopy and X-Ray diffraction (XRD). The laser-sintered GeSn films with 12% Sn exhibited a Raman peak at 295 cm^{-1} which is around 5 cm^{-1} left-shifted due to the high Sn concentration. The XRD 2θ peak of GeSn (111) and GeSn (220) were identified at an angle of 27.15° and 44.20°, which indicated the polycrystalline GeSn formation. The laser-sintered GeSn films showed hole mobility of 240 $cm^2/V.s$. Analyzing the optical characteristics, it was also found that the film would absorb almost 70% of the IR light in the near and mid-IR regions. The developed LS process allows the quick deposition of thick polycrystalline films, removing surface porosity and voids, increasing films adhesion with the substrate, and faster thermal annealing.

Keywords: polycrystalline GeSn, nanoparticle, laser sintering, crystallization, mobility, photodetector

Photoconductive PbSe Thin Films for Infrared Imaging

Mool C. Gupta[1], Joel T. Harrison, and Md Toriqul Islam[1]

[1]Department of Electrical and Computer Engineering, University of Virginia, Charlottesville, VA 22904, USA

Email: mg9re@virginia.edu

Abstract

Lead selenide (PbSe) emerged 70+ years ago for its unique photoconductive sensitivity to the mid-wave infrared (MWIR) spectrum; however, new and exciting research continues to ignite interest in this material to this day. PbSe has endured primarily due to its high IR responsivity at room temperature (uncooled), large-area application space, and low-cost fabrication. PbSe has a large nominal Bohr exciton radius (~46 nm) that allows bandgap tuning from 0.27 eV to as far as 2.0 eV by manipulation of grain size and morphology. This review aims to summarize the most recent state-of-the-art progress in PbSe photoconductivity research, including synthesized quantum dots (QDs) and novel manufacturing methods.

DOI: 10.1039/D0MA00965B (Review Article) *Mater. Adv.*, 2021, **2**, 3133-3160